arXiv:1008.3996v2 [hep-ex] 2 May 2011

Measurement of azimuthal asymmetries associated with deeply virtual Compton scattering on a longitudinally polarized deuterium target

The HERMES Collaboration

A. Airapetian [ℓ,o] N. Akopov [z] Z. Akopov [e] E.C. Aschenauer [f,1]
W. Augustyniak [y] R. Avakian [z] A. Avetissian [z] E. Avetisyan [e]
S. Belostotski [r] N. Bianchi [j] H.P. Blok [q,x] A. Borissov [e] J. Bowles [m]
I. Brodski [ℓ] V. Bryzgalov [s] J. Burns [m] M. Capiluppi [i] G.P. Capitani [j]
E. Cisbani [u] G. Ciullo [i] M. Contalbrigo [i] P.F. Dalpiaz [i] W. Deconinck [e,o,2]
R. De Leo [b] L. De Nardo [k,e] E. De Sanctis [j] M. Diefenthaler [n,h]
P. Di Nezza [j] M. Düren [ℓ] M. Ehrenfried [ℓ] G. Elbakian [z] F. Ellinghaus [d,3]
A. Fantoni [j] L. Felawka [v] S. Frullani [u] D. Gabbert [f] G. Gapienko [s]
V. Gapienko [s] F. Garibaldi [u] G. Gavrilov [e,r,v] V. Gharibyan [z]
F. Giordano [e,i] S. Gliske [o] M. Golembiovskaya [f] C. Hadjidakis [j]
M. Hartig [e,4] D. Hasch [j] G. Hill [m] A. Hillenbrand [f] M. Hoek [m] Y. Holler [e]
I. Hristova [f] Y. Imazu [w] A. Ivanilov [s] H.E. Jackson [a] A. Jgoun [r] H.S. Jo [k]
S. Joosten [n,k] R. Kaiser [m] G. Karyan [z] T. Keri [m,ℓ] E. Kinney [d] A. Kisselev [r]
N. Kobayashi [w] V. Korotkov [s] V. Kozlov [p] B. Krauss [h] P. Kravchenko [r]
V.G. Krivokhijine [g] L. Lagamba [b] R. Lamb [n] L. Lapikás [q] I. Lehmann [m]
P. Lenisa [i] L.A. Linden-Levy [n] A. López Ruiz [k] W. Lorenzon [o] X.-G. Lu [f]
X.-R. Lu [w] B.-Q. Ma [c] D. Mahon [m] N.C.R. Makins [n] S.I. Manaenkov [r]
L. Manfré [u] Y. Mao [c] B. Marianski [y] A. Martinez de la Ossa [d]
H. Marukyan [z] C.A. Miller [v] A. Movsisyan [z] V. Muccifora [j] M. Murray [m]
D. Müller [5] A. Mussgiller [e,h] E. Nappi [b] Y. Naryshkin [r] A. Nass [h]
M. Negodaev [f] W.-D. Nowak [f] L.L. Pappalardo [i] R. Perez-Benito [ℓ]
N. Pickert [h] M. Raithel [h] P.E. Reimer [a] A.R. Reolon [j] C. Riedl [f] K. Rith [h]
G. Rosner [m] A. Rostomyan [e] J. Rubin [n] D. Ryckbosch [k] Y. Salomatin [s]
F. Sanftl [t] A. Schäfer [t] G. Schnell [f,k] K.P. Schüler [e] B. Seitz [m]
T.-A. Shibata [w] V. Shutov [g] M. Stancari [i] M. Statera [i] E. Steffens [h]
J.J.M. Steijger [q] H. Stenzel [ℓ] J. Stewart [f] F. Stinzing [h] S. Taroian [z]

A. Terkulov [p] A. Trzcinski [y] M. Tytgat [k] A. Vandenbroucke [k]
P.B. Van der Nat [q] Y. Van Haarlem [k,6] C. Van Hulse [k] D. Veretennikov [r]
V. Vikhrov [r] I. Vilardi [b] C. Vogel [h] S. Wang [c] S. Yaschenko [f,h] Z. Ye [e]
S. Yen [v] W. Yu [ℓ] D. Zeiler [h] B. Zihlmann [e] P. Zupranski [y]

[a] *Physics Division, Argonne National Laboratory, Argonne, IL 60439-4843, USA*
[b] *Istituto Nazionale di Fisica Nucleare, Sezione di Bari, 70124 Bari,Italy*
[c] *School of Physics, Peking University, Beijing 100871, China*
[d] *Nuclear Physics Laboratory, University of Colorado, Boulder, CO 80309-0390, USA*
[e] *DESY, 22603 Hamburg, Germany*
[f] *DESY, 15738 Zeuthen, Germany*
[g] *Joint Institute for Nuclear Research, 141980 Dubna, Russia*
[h] *Physikalisches Institut, Universität Erlangen-Nürnberg, 91058 Erlangen, Germany*
[i] *Istituto Nazionale di Fisica Nucleare, Sezione di Ferrara and Dipartimento di Fisica, Università di Ferrara, 44100 Ferrara, Italy*
[j] *Istituto Nazionale di Fisica Nucleare, Laboratori Nazionali di Frascati, 00044 Frascati, Italy*
[k] *Department of Subatomic and Radiation Physics, University of Gent, 9000 Gent, Belgium*
[ℓ] *Physikalisches Institut, Universität Gießen, 35392 Gießen, Germany*
[m] *Department of Physics and Astronomy, University of Glasgow, Glasgow G12 8QQ, United Kingdom*
[n] *Department of Physics, University of Illinois, Urbana, IL 61801-3080, USA*
[o] *Randall Laboratory of Physics, University of Michigan, Ann Arbor, MI 48109-1040, USA*
[p] *Lebedev Physical Institute, 117924 Moscow, Russia*
[q] *National Institute for Subatomic Physics (Nikhef), 1009 DB Amsterdam, The Netherlands*
[r] *Petersburg Nuclear Physics Institute, Gatchina, Leningrad region 188300, Russia*
[s] *Institute for High Energy Physics, Protvino, Moscow region 142281, Russia*
[t] *Institut für Theoretische Physik, Universität Regensburg, 93040 Regensburg, Germany*
[u] *Istituto Nazionale di Fisica Nucleare, Sezione Roma 1, Gruppo Sanità and Physics Laboratory, Istituto Superiore di Sanità, 00161 Roma, Italy*
[v] *TRIUMF, Vancouver, British Columbia V6T 2A3, Canada*
[w] *Department of Physics, Tokyo Institute of Technology, Tokyo 152, Japan*
[x] *Department of Physics and Astronomy, VU University, 1081 HV Amsterdam, The Netherlands*
[y] *Andrzej Soltan Institute for Nuclear Studies, 00-689 Warsaw, Poland*
[z] *Yerevan Physics Institute, 375036 Yerevan, Armenia*

Abstract

Azimuthal asymmetries in exclusive electroproduction of a real photon from a longitudinally polarized deuterium target are measured with respect to target polarization alone and with respect to target polarization combined with beam helicity and/or beam charge. The asymmetries appear in the distribution of the real photons in the azimuthal angle ϕ around the virtual photon direction, relative to the lepton scattering plane. The asymmetries arise from the deeply virtual Compton scattering process and its interference with the Bethe-Heitler process. The results for the beam-charge and beam-helicity asymmetries from a tensor polarized deuterium target with vanishing vector polarization are shown to be compatible with those from an unpolarized deuterium target, which is expected for incoherent scattering dominant at larger momentum transfer. Furthermore, the results for the single target-spin asymmetry and for the double-spin asymmetry are found to be compatible with the corresponding asymmetries previously measured on a hydrogen target. For coherent scattering on the deuteron at small momentum transfer to the target, these findings imply that the tensor contribution to the cross section is small. Furthermore, the tensor asymmetry is found to be compatible with zero.

Key words: DIS, HERMES experiments, GPDs, DVCS, polarized deuterium target
PACS: 13.60.-r, 24.85.+p, 13.60.Fz, 14.20.Dh

1. Introduction

Generalized Parton Distributions (GPDs) provide a framework for describing the multidimensional structure of the nucleon [1–3]. GPDs encompass parton distribution functions and elastic nucleon form factors as limiting cases and moments, respectively. Parton distribution functions are distributions in longitudinal momentum fraction of partons in the nucleon, and are extracted from measurements of inclusive and semi-inclusive deep-inelastic scattering. Form factors are related to the transverse spatial distribution of charge and magnetization in the nucleon. Both form factors and (transverse-momentum-integrated) parton distribution functions represent one-dimensional distributions, whereas GPDs provide correlated information on transverse spatial and longitudinal momentum distributions of partons [4–9]. Furthermore, access to the total parton angular momentum contribution to the nucleon spin may be provided by GPDs through the Ji relation [3].

Hard exclusive leptoproduction of a meson or photon, with only an intact nucleon or nucleus remaining in the final state, can be described in terms of GPDs. GPDs depend on four kinematic variables: t, x, ξ, and Q^2. In this case, t is the Mandelstam variable, or the squared four-momentum transfer to the target, given by $t = (p - p')^2$, where p (p') is the initial (final) four-momentum of the target. In the 'infinite' target-momentum frame, x and ξ are related to the longitudinal momentum of the parton involved in the interaction as a fraction of the target momentum. The variable x is the average momentum fraction and the variable ξ, known as the skewness, is half the difference between the initial and final momentum fractions carried by the parton. The evolution of GPDs with $Q^2 \equiv -q^2$, with $q = k - k'$ the difference between the four-momenta of the incident and scattered leptons, can be calculated in the context of perturbative quantum chromodynamics as in the case of parton distribution functions. This evolution has been evaluated to leading order [1–3,10] and next-to-leading order [11–13] in the strong coupling constant α_s. The skewness ξ can be related to the Bjorken scaling variable $x_B \equiv Q^2/(2p \cdot q)$ through $\xi \simeq x_B/(2 - x_B)$ in the generalized Bjorken limit of large Q^2, and fixed x_B and t. There is currently no consensus as to how to define ξ in terms of experimental observables; hence the experimental results are typically reported as projections in x_B. The entire x dependences of GPDs are generally not experimentally accessible, an exception being the trajectory $x = \xi$ [14,15].

GPDs can be constrained through measurements of cross sections and asymmetries in exclusive processes such as exclusive photon or meson production. In this paper, the

[1] Now at: Brookhaven National Laboratory, Upton, NY 11772-5000, USA
[2] Now at: Massachusetts Institute of Technology, Cambridge, MA 02139, USA
[3] Now at: Institut für Physik, Universität Mainz, 55128 Mainz, Germany
[4] Now at: Institut für Kernphysik, Universität Frankfurt a.M., 60438 Frankfurt a.M., Germany
[5] Present address: Institut für Theoretische Physik II, Ruhr-Universität Bochum, 44780 Bochum, Germany
[6] Now at: Carnegie Mellon University, Pittsburgh, PA 15213, USA

Deeply Virtual Compton Scattering (DVCS) process, i.e., the hard exclusive production of a real photon, is investigated using a longitudinally polarized deuterium target.

The spin-1/2 nucleon is described by four leading-twist quark-chirality-conserving GPDs H, E, $\widetilde{H}$ and $\widetilde{E}$ [1–3,16]. In contrast, DVCS leaving the spin-1 deuteron intact requires nine GPDs: H_1, H_2, H_3, H_4, H_5, $\widetilde{H}_1$, $\widetilde{H}_2$, $\widetilde{H}_3$ and $\widetilde{H}_4$ [17–19]. In the forward limit of vanishing four-momentum transfer to the target nucleon ($t \to 0$ and $\xi \to 0$), the pairs of GPDs (H, H_1) and ($\widetilde{H}$, $\widetilde{H}_1$) reduce respectively to quark number density and helicity distributions. In this limit the GPD H_5, sensitive to tensor effects in the deuteron, reduces to the tensor structure function b_1, which was measured in inclusive deep-inelastic scattering on a tensor polarized deuterium target [20]. Both H_3 and H_5 are associated with the 5% D-wave component of the deuteron wave function in terms of nucleons [22]. In addition to GPD H_1, they both contribute to the beam-helicity and beam-charge asymmetries. The term with GPD H_5 dominates in the beam-helicity$\otimes$tensor asymmetry in DVCS from a longitudinally polarized deuterium target at very small values of t [18]. At this kinematic condition, the asymmetry with respect to target polarization is dominated by the term with GPD $\widetilde{H}_1$. Thus, the measurement of certain asymmetries in DVCS on a polarized deuterium target may provide new constraints for these GPDs.

This paper reports the first observation of azimuthal asymmetries with respect to target polarization alone and with respect to target polarization combined with beam helicity and/or beam charge, for exclusive electroproduction of real photons from a longitudinally polarized deuterium target. The asymmetries arise from the DVCS process where the photon is radiated by the struck quark, and its interference with the Bethe–Heitler (BH) process where the photon is radiated by the initial or final state lepton. The resulting asymmetries combine contributions from the coherent process $e\,d \to e\,d\,\gamma$, and the incoherent process $e\,d \to e\,p\,n\,\gamma$ where in addition a nucleon may be excited to a resonance. The coherent reaction contributes mainly at very small values of t, while the incoherent process dominates elsewhere. It is natural to model the incoherent process as scattering on only one nucleon in the deuteron, while the other nucleon acts as a spectator. Monte Carlo simulations in HERMES kinematic conditions [23] suggest that the proton contributes about 75% of the incoherent yield and the neutron about 25%, and included in these, nucleon resonance production contributes about 22% of the incoherent yield. The incoherent reaction on a proton dominates that on a neutron because of the suppression of the BH amplitude on the neutron by the small elastic electric form factor at low and moderate values of the momentum transfer to the target. The dependence of the measured asymmetries on the kinematic conditions of the reaction is also presented and these results on the deuteron are compared where appropriate with the corresponding results obtained on a longitudinally polarized hydrogen target [24].

2. Deeply virtual Compton scattering

2.1. *Scattering amplitudes*

The DVCS process is currently the simplest experimentally accessible process that can be used to constrain GPDs. The initial and final states of DVCS are indistinguishable from those of the competing BH process. For a target of atomic mass number A and no target polarization component transverse to the direction of the virtual photon, the

general expression for the cross section of the coherent reaction $e\,A \to e\,A\,\gamma$ or incoherent reaction $e\,A \to e\,(A-1)N\,\gamma$ reads [18,25]

$$\frac{\mathrm{d}\sigma}{\mathrm{d}x_A\,\mathrm{d}Q^2\,\mathrm{d}|t|\,\mathrm{d}\phi} = \frac{x_A\,e^6}{32\,(2\pi)^4\,Q^4}\,\frac{|\mathcal{T}|^2}{\sqrt{1+\varepsilon^2}}\,. \tag{1}$$

Here, $x_A \equiv Q^2/(2M_A\nu)$ is the nuclear Bjorken variable, where M_A is the mass of the nucleus and $\nu \equiv p\cdot q/M_A$, e is the elementary charge, $\varepsilon \equiv 2x_A M_A/\sqrt{Q^2}$ and $\mathcal{T}$ is the reaction amplitude. The azimuthal angle of the real photon around the virtual-photon direction, relative to the lepton scattering plane, is denoted by ϕ. The cross section contains the coherent superposition of BH and DVCS amplitudes:

$$|\mathcal{T}|^2 = |\mathcal{T}_{\mathrm{BH}} + \mathcal{T}_{\mathrm{DVCS}}|^2 = |\mathcal{T}_{\mathrm{BH}}|^2 + |\mathcal{T}_{\mathrm{DVCS}}|^2 + \underbrace{\mathcal{T}_{\mathrm{DVCS}}\,\mathcal{T}^*_{\mathrm{BH}} + \mathcal{T}^*_{\mathrm{DVCS}}\,\mathcal{T}_{\mathrm{BH}}}_{\mathrm{I}}\,, \tag{2}$$

where 'I' denotes the BH-DVCS interference term. The BH amplitude is calculable to leading order in QED using the form factors measured in elastic scattering.

The interference term I and the squared DVCS amplitude $|\mathcal{T}_{\mathrm{DVCS}}|^2$ in Eq. 2 provide experimental access to the (complex) DVCS amplitude through measurements of various cross section asymmetries as functions of ϕ [18]. Each of the three terms of Eq. 2 can be written as a Fourier series in ϕ. In the case that the beam and the target may be longitudinally polarized, these terms read

$$|\mathcal{T}_{\mathrm{BH}}|^2 = \frac{K_{\mathrm{BH}}}{\mathcal{P}_1(\phi)\mathcal{P}_2(\phi)} \times \sum_{n=0}^{2} c_n^{\mathrm{BH}}\cos(n\phi)\,, \tag{3}$$

$$|\mathcal{T}_{\mathrm{DVCS}}|^2 = K_{\mathrm{DVCS}} \times \left\{ \sum_{n=0}^{2} c_n^{\mathrm{DVCS}}\cos(n\phi) + \sum_{n=1}^{2} s_n^{\mathrm{DVCS}}\sin(n\phi) \right\}, \tag{4}$$

$$\mathrm{I} = -\frac{e_\ell K_{\mathrm{I}}}{\mathcal{P}_1(\phi)\mathcal{P}_2(\phi)} \times \left\{ \sum_{n=0}^{3} c_n^{\mathrm{I}}\cos(n\phi) + \sum_{n=1}^{3} s_n^{\mathrm{I}}\sin(n\phi) \right\}. \tag{5}$$

The symbols $K_{\mathrm{BH}} = \frac{1}{x_A^2\,t\,(1+\varepsilon^2)^2}$, $K_{\mathrm{DVCS}} = \frac{1}{Q^2}$ and $K_{\mathrm{I}} = \frac{1}{x_A\,y\,t}$ denote kinematic factors, where $y \equiv p\cdot q/(p\cdot k)$, and e_ℓ stands for the (signed) lepton charge in units of the elementary charge. In the case of unpolarized beam and target, certain coefficients vanish. All Fourier coefficients c_n and s_n in Eqs. 3–5 depend on the longitudinal target polarization, with some also having a dependence on the beam helicity. The coefficients c_n^{BH} in Eq. 3 depend on electromagnetic form factors of the target, while the DVCS (interference) coefficients c_n^{DVCS} (c_n^{I}) and s_n^{DVCS} (s_n^{I}) involve various GPDs. The squared BH and interference terms in Eqs. 3 and 5 have an additional ϕ dependence in the denominator due to the lepton propagators $\mathcal{P}_1(\phi)$ and $\mathcal{P}_2(\phi)$ [25,16]. The Fourier coefficients c_n^{I} and s_n^{I} in Eq. 5 can be expressed as linear combinations of Compton Form Factors (CFFs) [18], while the coefficients c_n^{DVCS} and s_n^{DVCS} are bilinear in the CFFs. Such CFFs are convolutions of the corresponding GPDs with the hard scattering coefficient functions.

For a longitudinally (L) polarized lepton beam scattered from an unpolarized target, the beam-charge asymmetry $\mathcal{A}_{\mathrm{C}}$ and the *charge-difference* beam-helicity asymmetry $\mathcal{A}_{\mathrm{LU}}^{\mathrm{I}}$ (sensitive to the interference term) and *charge-average* beam-helicity asymmetry $\mathcal{A}_{\mathrm{LU}}^{\mathrm{DVCS}}$ (sensitive to the squared DVCS term) can be measured if all four combinations

of beam charge and helicity are available [26]. Results of their Fourier amplitudes for an unpolarized deuterium target were recently published by HERMES [27].

Unfortunately, the present data set for a longitudinally polarized target does not include all four combinations of beam charge and sign of beam polarization. Therefore, the beam-helicity asymmetries presented in this paper are *single-charge* observables, which entangle the interference and squared DVCS term. Fortunately, measurements of *charge-averaged* beam-helicity asymmetries on hydrogen [26] and deuterium [27] targets showed that the contribution by the squared DVCS term is negligible in HERMES kinematic conditions, at the precision of these measurements.

2.2. *DVCS on the deuteron*

For coherent scattering on a spin-1 target nucleus polarized longitudinally with respect to the virtual photon direction, and with spin projection $\Lambda = \pm 1, 0$, the following decomposition of the Fourier coefficients appearing in Eqs. 3–5 is introduced [18]:

$$c_n^{\mathrm{R}}(\Lambda) = \frac{3}{2}\Lambda^2 c_{n,\mathrm{unp}}^{\mathrm{R}} + \Lambda c_{n,\mathrm{LP}}^{\mathrm{R}} + (1 - \frac{3}{2}\Lambda^2) c_{n,\mathrm{LLP}}^{\mathrm{R}} \tag{6}$$

with $\mathrm{R} \in \{\mathrm{BH}, \mathrm{DVCS}, \mathrm{I}\}$, and similarly for the s_n coefficients with $\mathrm{R} \in \{\mathrm{DVCS}, \mathrm{I}\}$. The subscript 'unp' denotes unpolarized and 'LP' and 'LLP' denote respectively vector and tensor terms for parts of the cross section related to longitudinal polarization. For an unpolarized target nucleus, one recovers the value $[c_n^{\mathrm{R}}(\Lambda = -1) + c_n^{\mathrm{R}}(\Lambda = 0) + c_n^{\mathrm{R}}(\Lambda = +1)]/3 = c_{n,\mathrm{unp}}^{\mathrm{R}}$. A purely tensor-polarized target nucleus with $\Lambda = 0$ results in $c_n^{\mathrm{R}} = c_{n,\mathrm{LLP}}^{\mathrm{R}}$, while for $\Lambda \neq 0$ all coefficients contribute.

Equation 6 is applicable only for purely polarized states with $\Lambda = \pm 1, 0$. In a real experiment, the longitudinally polarized deuterium target contains a mixture of these pure polarized states, characterized by vector and tensor polarizations P_z and P_{zz} defined as

$$P_z = \frac{n^+ - n^-}{n^+ + n^- + n^0}\,, \quad P_{zz} = \frac{n^+ + n^- - 2n^0}{n^+ + n^- + n^0}\,, \tag{7}$$

where n^+, n^- and n^0 are the populations of the state with $\Lambda = +1$, -1 and 0, respectively.

For a lepton beam with given longitudinal beam polarization P_ℓ scattering coherently on a deuterium target with given vector and tensor polarizations P_z and P_{zz}, the Fourier series of the squared reaction amplitude reads, using the spin decompositions of Eq. 6,

$$|\mathcal{T}_{\rm BH}|^2 = \frac{K_{\rm BH}}{\mathcal{P}_1(\phi)\mathcal{P}_2(\phi)}\Bigg\{\sum_{n=0}^{2} c^{\rm BH}_{n,\rm unp}\cos(n\phi) + P_z P_\ell \sum_{n=0}^{1} c^{\rm BH}_{n,\rm LP}\cos(n\phi) + \frac{1}{2}P_{zz}\sum_{n=0}^{2}(c^{\rm BH}_{n,\rm unp} - c^{\rm BH}_{n,\rm LLP})\cos(n\phi)\Bigg\}, \tag{8}$$

$$|\mathcal{T}_{\rm DVCS}|^2 = K_{\rm DVCS}\Bigg\{\sum_{n=0}^{2} c^{\rm DVCS}_{n,\rm unp}\cos(n\phi) + P_\ell\, s^{\rm DVCS}_{1,\rm unp}\sin\phi + P_z\Bigg[P_\ell\sum_{n=0}^{1} c^{\rm DVCS}_{n,\rm LP}\cos(n\phi) + \sum_{n=1}^{2} s^{\rm DVCS}_{n,\rm LP}\sin(n\phi)\Bigg] + \frac{1}{2}P_{zz}\Bigg[\sum_{n=0}^{2}(c^{\rm DVCS}_{n,\rm unp} - c^{\rm DVCS}_{n,\rm LLP})\cos(n\phi) + P_\ell\,(s^{\rm DVCS}_{1,\rm unp} - s^{\rm DVCS}_{1,\rm LLP})\sin\phi\Bigg]\Bigg\}, \tag{9}$$

$$\mathrm{I} = -\frac{e_\ell K_{\rm I}}{\mathcal{P}_1(\phi)\mathcal{P}_2(\phi)}\Bigg\{\sum_{n=0}^{3} c^{\rm I}_{n,\rm unp}\cos(n\phi) + P_\ell\sum_{n=1}^{2} s^{\rm I}_{n,\rm unp}\sin(n\phi) + P_z\Bigg[P_\ell\sum_{n=0}^{2} c^{\rm I}_{n,\rm LP}\cos(n\phi) + \sum_{n=1}^{3} s^{\rm I}_{n,\rm LP}\sin(n\phi)\Bigg] + \frac{1}{2}P_{zz}\Bigg[\sum_{n=0}^{3}(c^{\rm I}_{n,\rm unp} - c^{\rm I}_{n,\rm LLP})\cos(n\phi) + P_\ell\sum_{n=1}^{2}(s^{\rm I}_{n,\rm unp} - s^{\rm I}_{n,\rm LLP})\sin(n\phi)\Bigg]\Bigg\}. \tag{10}$$

Note that the beam polarization P_ℓ and the target vector and tensor polarizations P_z and P_{zz} are here factored out of the corresponding Fourier coefficients in Eqs. 3–5, thus leaving only the dynamical kinematic dependences encoded in the Fourier coefficients in Eqs. 8–10.

2.3. *Asymmetries on the deuteron*

For data with longitudinal polarization of both beam and target, the following notation is introduced: $\rightarrow$ ($\leftarrow$) to denote positive (negative) beam helicity, and $\Rightarrow$ and $\Leftarrow$ to denote the deuteron target vector-polarization direction anti-parallel and parallel to the beam momentum direction in the target rest frame. In contrast to lepton scattering off longitudinally polarized hydrogen [24], there are many more observables (asymmetries) in the case of deuterium. They may be classified according to whether the cross section for $\Lambda = 0$ explicitly appears in the definition of this asymmetry. An example of the 'incomplete' asymmetries where it does not appear is the beam-helicity asymmetry $\mathcal{A}_{\mathrm{L}\overrightarrow{\Leftarrow}}(e_\ell, P_{zz}, \phi)$, defined for beam charge e_ℓ and tensor polarization P_{zz} as

$$\mathcal{A}_{\mathrm{L}\overrightarrow{\Leftarrow}}(e_\ell, P_{zz}, \phi) \equiv \frac{\left[\mathrm{d}\sigma^{\overrightarrow{\Rightarrow}}(e_\ell, P_{zz}, \phi) + \mathrm{d}\sigma^{\overrightarrow{\Leftarrow}}(e_\ell, P_{zz}, \phi)\right] - \left[\mathrm{d}\sigma^{\overleftarrow{\Rightarrow}}(e_\ell, P_{zz}, \phi) + \mathrm{d}\sigma^{\overleftarrow{\Leftarrow}}(e_\ell, P_{zz}, \phi)\right]}{\left[\mathrm{d}\sigma^{\overrightarrow{\Rightarrow}}(e_\ell, P_{zz}, \phi) + \mathrm{d}\sigma^{\overrightarrow{\Leftarrow}}(e_\ell, P_{zz}, \phi)\right] + \left[\mathrm{d}\sigma^{\overleftarrow{\Rightarrow}}(e_\ell, P_{zz}, \phi) + \mathrm{d}\sigma^{\overleftarrow{\Leftarrow}}(e_\ell, P_{zz}, \phi)\right]}. \tag{11}$$

Here, the symbol '$\mathrm{d}\sigma$' denotes a generic differential cross section.

For coherent scattering, and to leading order in α_s and in leading twist, the expansion in powers of the Bjorken variable x_D for the deuteron target, and $\tau = t/(4M_D^2)$, where M_D is the deuteron mass, yields [18]

$$\mathcal{A}_{\mathrm{L}\overleftrightarrows}(e_\ell, P_{zz}=+1,\phi) \simeq -e_\ell \frac{x_D(2-y)\sqrt{\frac{-t}{Q^2}(1-y)}}{2-2y+y^2}\sin\phi$$
$$\times\, \Im\mathrm{m}\frac{G_1\mathcal{H}_1 - \frac{1}{3}G_1\mathcal{H}_5 - \tau\Big[G_1\mathcal{H}_3 + G_3(\mathcal{H}_1 - \frac{1}{3}\mathcal{H}_5)\Big] + 2\tau^2 G_3\mathcal{H}_3}{G_1^2 - 2\tau G_1 G_3 + 2\tau^2 G_3^2} \tag{12}$$
$$\simeq -e_\ell \frac{x_D(2-y)\sqrt{\frac{-t}{Q^2}(1-y)}}{2-2y+y^2}\frac{\Im\mathrm{m}(\mathcal{H}_1 - \frac{1}{3}\mathcal{H}_5)}{G_1}\sin\phi\,. \tag{13}$$

Here, G_1 and G_3 are deuteron elastic form factors [28]. (For comparison with experimental data, the actual value of $P_{zz} \neq 1$ must be taken into account in, e.g., Eqs. 12, 13, and those that follow.) Equation 13 is obtained neglecting the contributions of non-leading terms in τ in Eq. 12, which are less than 10% at $-t < 0.03\,\mathrm{GeV}^2$ (see Fig. 3 in Ref. [27]). As can be seen from Eqs. 12 and 13, this asymmetry involves a different linear combination of the imaginary parts of the deuteron CFFs $\mathcal{H}_1$, $\mathcal{H}_3$ and $\mathcal{H}_5$ compared to the asymmetry $\mathcal{A}_{\mathrm{LU}}^{\mathrm{I}}(\phi)$ (see Eqs. 25-27 in Ref. [27]). More specifically, any difference between these two asymmetries at small values of $-t$ may be ascribed to the CFF $\mathcal{H}_5$. Detailed information about the relations between these CFFs and corresponding GPDs can be found in Ref. [18].

Similarly, the beam-charge asymmetry for tensor polarization P_{zz} is defined as

$$\mathcal{A}_{\mathrm{C}\overleftrightarrows}(P_{zz},\phi) \equiv \frac{\Big[\mathrm{d}\sigma^{\overset{+}{\Rightarrow}}(P_{zz},\phi) + \mathrm{d}\sigma^{\overset{+}{\Leftarrow}}(P_{zz},\phi)\Big] - \Big[\mathrm{d}\sigma^{\overset{-}{\Rightarrow}}(P_{zz},\phi) + \mathrm{d}\sigma^{\overset{-}{\Leftarrow}}(P_{zz},\phi)\Big]}{\Big[\mathrm{d}\sigma^{\overset{+}{\Rightarrow}}(P_{zz},\phi) + \mathrm{d}\sigma^{\overset{+}{\Leftarrow}}(P_{zz},\phi)\Big] + \Big[\mathrm{d}\sigma^{\overset{-}{\Rightarrow}}(P_{zz},\phi) + \mathrm{d}\sigma^{\overset{-}{\Leftarrow}}(P_{zz},\phi)\Big]}\,, \tag{14}$$

where the symbols + (−) denote positive (negative) beam charge. For coherent scattering, the $\cos\phi$ component in the kinematic expansion of Eq. 14 is sensitive to the real part of the same linear combination of CFFs as that appearing in Eq. 13:

$$\mathcal{A}_{\mathrm{C}\overleftrightarrows}(P_{zz}=+1,\phi) \simeq -\frac{x_D\sqrt{\frac{-t}{Q^2}(1-y)}}{y}\frac{\Re\mathrm{e}(\mathcal{H}_1 - \frac{1}{3}\mathcal{H}_5)}{G_1}\cos\phi\ . \tag{15}$$

The different sign of the asymmetry $\mathcal{A}_{\mathrm{C}\overleftrightarrows}(P_{zz}=+1,\phi)$ compared to Ref. [18] is due to the use of the Trento convention [29] in this work, i.e., $\phi = \pi - \phi_{[18]}$.

Another single-charge beam-helicity asymmetry, which differs from $\mathcal{A}_{\mathrm{L}\overleftrightarrows}(e_\ell, P_{zz}, \phi)$ and $\mathcal{A}_{\mathrm{C}\overleftrightarrows}(e_\ell, P_{zz}, \phi)$, involves polarized beam and (longitudinal) tensor polarization of the deuteron:

$$\mathcal{A}_{\mathrm{Lzz}}(e_\ell,\phi) \equiv \frac{\mathrm{d}\sigma_{\mathrm{zz}}^{\rightarrow}(e_\ell,\phi) - \mathrm{d}\sigma_{\mathrm{zz}}^{\leftarrow}(e_\ell,\phi)}{3\mathrm{d}\sigma_{\mathrm{unp}}^{\rightarrow}(e_\ell,\phi) + 3\mathrm{d}\sigma_{\mathrm{unp}}^{\leftarrow}(e_\ell,\phi)}\,, \tag{16}$$

with $\mathrm{d}\sigma_{\mathrm{zz}} = \mathrm{d}\sigma^{\Rightarrow} + \mathrm{d}\sigma^{\Leftarrow} - 2\mathrm{d}\sigma^0$ and $\mathrm{d}\sigma_{\mathrm{unp}} = \frac{1}{3}(\mathrm{d}\sigma^{\Rightarrow} + \mathrm{d}\sigma^{\Leftarrow} + \mathrm{d}\sigma^0)$, where $\mathrm{d}\sigma^0$ represents the cross section for deuterons in the $\Lambda = 0$ state. For coherent scattering, the asymmetry $\mathcal{A}_{\mathrm{Lzz}}(e_\ell,\phi)$ involves a different linear combination of the imaginary parts of the deuteron CFFs $\mathcal{H}_1$, $\mathcal{H}_3$ and $\mathcal{H}_5$ compared to $\mathcal{A}_{\mathrm{L}\overleftrightarrows}(e_\ell, P_{zz}=+1,\phi)$ and $\mathcal{A}_{\mathrm{LU}}^{\mathrm{I}}(\phi)$:

$$\mathcal{A}_{\mathrm{Lzz}}(e_\ell,\phi) \simeq e_\ell \frac{2x_D(2-y)\sqrt{\frac{-t}{Q^2}(1-y)}}{2-2y+y^2}\sin\phi$$
$$\times\, \Im\mathrm{m}\frac{G_1\mathcal{H}_5 + \tau\left(G_1\mathcal{H}_3 + G_3\mathcal{H}_1 - \frac{1}{3}G_3\mathcal{H}_5\right) - 2\tau^2 G_3\mathcal{H}_3}{3G_1^2 - 4\tau G_1 G_3 + 4\tau^2 G_3^2} \tag{17}$$
$$\simeq e_\ell \frac{2x_D(2-y)\sqrt{\frac{-t}{Q^2}(1-y)}}{2-2y+y^2}\frac{\Im\mathrm{m}\mathcal{H}_5}{3G_1}\sin\phi\,. \tag{18}$$

Finally, the single-charge asymmetry with respect to longitudinal vector polarization of the target is defined as

$$\mathcal{A}_{\mathrm{UL}}(e_\ell, P_{zz}, \phi) \equiv$$
$$\frac{\left[\mathrm{d}\sigma^{\vec{\Rightarrow}}(e_\ell,P_{zz},\phi) + \mathrm{d}\sigma^{\overleftarrow{\Rightarrow}}(e_\ell,P_{zz},\phi)\right] - \left[\mathrm{d}\sigma^{\vec{\Leftarrow}}(e_\ell,P_{zz},\phi) + \mathrm{d}\sigma^{\overleftarrow{\Leftarrow}}(e_\ell,P_{zz},\phi)\right]}{\left[\mathrm{d}\sigma^{\vec{\Rightarrow}}(e_\ell,P_{zz},\phi) + \mathrm{d}\sigma^{\overleftarrow{\Rightarrow}}(e_\ell,P_{zz},\phi)\right] + \left[\mathrm{d}\sigma^{\vec{\Leftarrow}}(e_\ell,P_{zz},\phi) + \mathrm{d}\sigma^{\overleftarrow{\Leftarrow}}(e_\ell,P_{zz},\phi)\right]}\,. \tag{19}$$

For coherent scattering, in analogy to the previously elaborated asymmetries, it reduces to

$$\mathcal{A}_{\mathrm{UL}}(e_\ell, P_{zz}=+1, \phi) \simeq -e_\ell \frac{x_D\,\sqrt{\frac{-t}{Q^2}(1-y)}}{y}\sin\phi$$
$$\times\, \Im\mathrm{m}\frac{\left[G_1\widetilde{\mathcal{H}}_1 + \frac{x_D}{2}\,G_2\left(\mathcal{H}_1 - \frac{1}{3}\mathcal{H}_5\right)\right] - \tau\left(G_3\widetilde{\mathcal{H}}_1 + \frac{x_D}{2}\,G_2\mathcal{H}_3\right)}{G_1^2 - 2\tau G_1 G_3 + 2\tau^2 G_3^2} \tag{20}$$
$$\simeq -e_\ell \frac{x_D\,\sqrt{\frac{-t}{Q^2}(1-y)}}{y}\frac{\Im\mathrm{m}\left[G_1\widetilde{\mathcal{H}}_1 + \frac{x_D}{2}\,G_2\left(\mathcal{H}_1 - \frac{1}{3}\mathcal{H}_5\right)\right]}{G_1^2}\sin\phi\,. \tag{21}$$

Thus, this asymmetry is sensitive to the imaginary part of the Compton form factor $\widetilde{\mathcal{H}}_1$.

3. The HERMES experiment

A detailed description of the HERMES spectrometer can be found in Ref. [30]. A longitudinally polarized positron or electron beam of energy 27.6 GeV was scattered off a longitudinally polarized deuterium gas target internal to the HERA lepton storage ring at DESY. The lepton beam was transversely self-polarized by the emission of synchrotron radiation [31]. Longitudinal polarization of the beam at the target was achieved by a pair of spin rotators in front of and behind the experiment [32]. The sign of the beam polarization was reversed approximately every two months. Two Compton backscattering polarimeters [33,34] measured independently the longitudinal and transverse beam polarizations. The average values of the beam polarization for the various running periods are given in Table 1; their average fractional systematic uncertainty is 2.2%.

The target cell was filled with nuclear-polarized atoms from an atomic beam source based on Stern–Gerlach separation with radio-frequency hyperfine transitions [35]. The polarization and atomic fraction of the target gas were continuously monitored [36,37]. Most of the longitudinally polarized deuterium data were recorded with average vector polarizations 0.851 ± 0.031 and -0.840 ± 0.028, and with an average tensor polarization

Table 1
The sign of the beam charge, the luminosity-averaged beam polarization and target vector and tensor polarization values, for the years 1998-2000 and the integrated luminosity of the data sets used for the extraction of the various asymmetry amplitudes (see Table 3) on a longitudinally polarized deuterium target. The uncertainties for the polarizations are given in the text.

Year	Lepton Charge	Beam Polarization	Target Polarization		Luminosity [pb^{-1}]		
			P_z	P_{zz}	$\mathcal{A}_{\mathrm{L}\overleftrightarrows}$ ($\mathcal{A}_{\mathrm{UL}}$, $\mathcal{A}_{\mathrm{LL}}$)	$\mathcal{A}_{\mathrm{C}\overleftarrow{\rightleftarrows}}$ ($\mathcal{A}_{0\overleftarrow{\mathrm{L}}}$, $\mathcal{A}_{\mathrm{C}\overleftarrow{\mathrm{L}}}$)	$\mathcal{A}_{\mathrm{Lzz}}$
1998	e^-	-0.509	± 0.856	$+0.827$		26.2	
1999	e^+	$-0.547, +0.518$	± 0.832	$+0.827$	29.7	14.2	29.7
2000	e^+	$-0.537, +0.524$	$-0.840, +0.851$	$+0.827$	125.8	43.5	125.8
2000	e^+	$-0.542, +0.525$	-0.010	-1.656			22.7
Sum					155.5	83.9	178.2

Table 2
The integrated luminosity of the data used for the extraction of various asymmetry amplitudes (see Table 3) on a longitudinally polarized deuterium target for each lepton beam charge and sign of the polarization.

Lepton Charge	Sign of the Beam Polarization	Luminosity [pb^{-1}]
e^-	negative	26.2
e^-	positive	
e^+	negative	75.4
e^+	positive	102.8

of 0.827 ± 0.027 [38] (corresponding to a small population of the $\Lambda = 0$ state). The extraction of $\mathcal{A}_{\mathrm{Lzz}}(\phi)$ employed the fraction of the data taken in the year 2000 recorded with a tensor-polarized deuterium target where deuterons in the $\Lambda = 0$ state were injected into the target cell, resulting in an average tensor polarization of -1.656 ± 0.049 with negligible vector polarization (-0.010 ± 0.026). The amount of data accumulated for each lepton beam charge and sign of the polarization are summarized in Table 2.

The scattered leptons and produced particles were detected by the HERMES spectrometer in the polar angle range 0.04 rad $< \theta <$ 0.22 rad. The average lepton identification efficiency was at least 98% with hadron contamination of less than 1%.

4. Event selection

The data sets used in the extraction of the various asymmetries reported here are given in Table 1. In this analysis, it was required that events contain exactly one charged-particle track identified as a lepton with the same charge as the beam lepton, and one photon producing an energy deposition $E_\gamma > 5\,\mathrm{GeV}$ ($> 1\,\mathrm{MeV}$) in the calorimeter (preshower detector). The following kinematic requirements were imposed on the events, as calculated from the four-momenta of the incoming and outgoing lepton: $1\,\mathrm{GeV}^2 < Q^2 < 10\,\mathrm{GeV}^2$, $W_N^2 > 9\,\mathrm{GeV}^2$, $\nu < 22\,\mathrm{GeV}$ and $0.03 < x_N < 0.35$, where $W_N^2 = M_N^2 + 2M_N\nu - Q^2$ and $x_N = Q^2/(2M_N\nu)$. For the nucleonic mass M_N, the proton mass

was used in all kinematic constraints on event selection, even at small values of $-t$ where coherent reactions on the deuteron are dominant, because the experiment does not distinguish between coherent and incoherent scattering and the latter dominates over most of the kinematic range. Monte Carlo studies have shown that this choice has little effect on the result [23]. In order to reduce background from the decay of neutral mesons, the angle between the laboratory three-momenta of the real and virtual photons was limited to $\theta_{\gamma^*\gamma} < 45\,\mathrm{mrad}$. The minimum angle requirement $\theta_{\gamma^*\gamma} > 5\,\mathrm{mrad}$ was chosen according to Monte Carlo simulations in order to ensure that the azimuthal angle ϕ remains well-defined while accounting for the finite angular resolution of the spectrometer.

An 'exclusive' event sample was selected by requiring the squared missing mass M_X^2 to be close to the squared nucleon mass M_N^2, where M_X^2 is defined as $M_X^2 = (q + P_N - q')^2$ with $P_N = (M_N, 0, 0, 0)$ and q' the four-momentum of the real photon. The exclusive region is defined as $-(1.5)^2\,\mathrm{GeV}^2 < M_X^2 < (1.7)^2\,\mathrm{GeV}^2$ to minimize background from deep-inelastic scattering fragmentation processes, while maintaining reasonable efficiency [39].

As the recoiling target nucleon or nucleus was undetected, the Mandelstam variable t was reconstructed from the measured four-momenta of the scattered lepton and the detected photon. The resolution in the photon energy from the calorimeter is inadequate for a precise determination of t. Hence for events selected in the exclusive region in M_X^2, the reaction is assumed to take place on a nucleon and the final state is assumed to contain only the scattered lepton, the real photon and the nucleon that was left intact ($e\,N \to e\,N\,\gamma$). This allows t to be calculated with improved resolution using only the photon direction and the lepton four-momentum [40]:

$$t = \frac{-Q^2 - 2\,\nu\,(\nu - \sqrt{\nu^2 + Q^2}\,\cos\theta_{\gamma^*\gamma})}{1 + \frac{1}{M_N}\,(\nu - \sqrt{\nu^2 + Q^2}\,\cos\theta_{\gamma^*\gamma})}\,. \tag{22}$$

The error caused by applying this expression to incoherent events with a nucleon excited to a resonance in the final state is accounted for in the Monte Carlo simulation that is used to calculate the fractional contribution of background processes per kinematic bin. This simulation also demonstrated that this method is applicable also to coherent events. A further restriction, $-t < 0.7\,\mathrm{GeV}^2$, is used in the selection of exclusive events in order to reduce background.

The exclusive sample comprises coherent and incoherent scattering, including resonance excitation. Over most of the kinematic range incoherent scattering dominates. The events from coherent scattering off the deuteron are concentrated at small values of $-t$. The Monte Carlo simulation showed that requiring $-t < 0.06\,\mathrm{GeV}^2$ enhances the relative contribution of the coherent process from 20% to 40% in the data sample. Requiring $-t < 0.01\,\mathrm{GeV}^2$ can further enhance the coherent contribution to 66%, but only at the cost of a rapidly decreasing yield. The first bin defined in Section 7 covering the range $-t < 0.06\,\mathrm{GeV}^2$ is sensitive to coherent effects.

5. Extraction formalism

The simultaneous extraction of Fourier amplitudes of beam-charge and beam-helicity asymmetries combining data collected during various running periods at HERMES for both beam charges and helicities on unpolarized hydrogen or deuterium targets is described in Refs. [27,26]. It is based on the maximum likelihood technique [41], which

provides a bin-free fit in the azimuthal angle ϕ (see Ref. [42] for details). In this paper, data taken with a longitudinally polarized deuterium target were analyzed with a similar technique. In the fit, event weights were introduced to account for luminosity imbalances with respect to beam charge and polarization.

Because the target polarization was longitudinal with respect to the direction of the incoming beam, the data also contain contributions arising from the small transverse polarization with respect to the direction of the virtual photon. This $6\% - 12\%$ transverse component of the target polarization, depending on the kinematic conditions of each bin, was neglected in the formalism presented. Hence, the extracted Fourier components contain contributions from this transverse component. However, mainly non-leading (higher-twist) amplitudes are affected by this choice. These effects are estimated from the measurement of the transverse-target-spin asymmetries at HERMES [42] to be less than 0.008 on a proton target, and hence are expected to be negligible compared with the uncertainties here.

5.1. *Single-charge formalism*

Data collected with an e^- beam and a polarized deuterium target were not used for the extraction of harmonics of $\mathcal{A}_{\mathrm{L}\overleftrightarrows}$, $\mathcal{A}_{\mathrm{UL}}$ and $\mathcal{A}_{\mathrm{LL}}$ because only negative beam polarization is available for this charge. Hence, Fourier amplitudes of the three *single-charge* asymmetries $\mathcal{A}_{\mathrm{L}\overleftrightarrows}(e_\ell = +1, P_{zz}, \phi)$, $\mathcal{A}_{\mathrm{UL}}(e_\ell = +1, P_{zz}, \phi)$ and $\mathcal{A}_{\mathrm{LL}}(e_\ell = +1, P_{zz}, \phi)$, defined respectively in Eqs. 11, 19, and 30, are simultaneously extracted using data from scattering of a longitudinally polarized positron beam off a longitudinally polarized deuterium target.

The distribution in the expectation value of the yield can be written as

$$\begin{aligned}
\mathrm{d}\langle\mathcal{N}\rangle(e_\ell = +1, P_\ell, P_z, P_{zz}, \phi) &= \mathcal{L}\,(e_\ell = +1, P_\ell, P_z, P_{zz})\,\eta(\phi) \\
&\times \mathrm{d}\sigma_{\mathrm{U}\overleftrightarrows}(e_\ell = +1, P_{zz}, \phi)\Big[1 + P_\ell \mathcal{A}_{\mathrm{L}\overleftrightarrows}(e_\ell = +1, P_{zz}, \phi) \\
&+ P_z \mathcal{A}_{\mathrm{UL}}(e_\ell = +1, P_{zz}, \phi) + P_\ell P_z \mathcal{A}_{\mathrm{LL}}(e_\ell = +1, P_{zz}, \phi)\Big], \quad (23)
\end{aligned}$$

where $\mathcal{L}$ denotes the integrated luminosity and η the detection efficiency. The cross section for the production of real photons by *unpolarized* positrons on a tensor-polarized deuterium target with vanishing vector polarization is given by

$$\begin{aligned}
\mathrm{d}\sigma_{\mathrm{U}\overleftrightarrows}(e_\ell = +1, P_{zz}, \phi) &\equiv \frac{1}{4}\Big[\mathrm{d}\sigma^{\overrightarrow{\Rightarrow}+}(P_{zz}, \phi) + \mathrm{d}\sigma^{\overleftarrow{\Leftarrow}+}(P_{zz}, \phi) \\
&\quad + \mathrm{d}\sigma^{\overleftarrow{\Rightarrow}+}(P_{zz}, \phi) + \mathrm{d}\sigma^{\overrightarrow{\Leftarrow}+}(P_{zz}, \phi)\Big] \quad (24) \\
&= K\Bigg\{\frac{K_{\mathrm{BH}}}{\mathcal{P}_1(\phi)\mathcal{P}_2(\phi)}\Big[\sum_{n=0}^{2} c^{\mathrm{BH}}_{n,\mathrm{unp}}\cos(n\phi) + \frac{1}{2}P_{zz}\sum_{n=0}^{2}(c^{\mathrm{BH}}_{n,\mathrm{unp}} - c^{\mathrm{BH}}_{n,\mathrm{LLP}})\cos(n\phi)\Big] \\
&+ K_{\mathrm{DVCS}}\Big[\sum_{n=0}^{2} c^{\mathrm{DVCS}}_{n,\mathrm{unp}}\cos(n\phi) + \frac{1}{2}P_{zz}\sum_{n=0}^{2}(c^{\mathrm{DVCS}}_{n,\mathrm{unp}} - c^{\mathrm{DVCS}}_{n,\mathrm{LLP}})\cos(n\phi)\Big] \\
&- \frac{K_{\mathrm{I}}}{\mathcal{P}_1(\phi)\mathcal{P}_2(\phi)}\Big[\sum_{n=0}^{3} c^{\mathrm{I}}_{n,\mathrm{unp}}\cos(n\phi) + \frac{1}{2}P_{zz}\sum_{n=0}^{3}(c^{\mathrm{I}}_{n,\mathrm{unp}} - c^{\mathrm{I}}_{n,\mathrm{LLP}})\cos(n\phi)\Big]\Bigg\}, \quad (25)
\end{aligned}$$

where $K = \frac{x_D\, e^6}{32\,(2\pi)^4\, Q^4 \sqrt{1+\varepsilon^2}}$ is a common kinematic factor.

The single-charge asymmetries appearing in Eq. 23 are expanded in terms of the same Fourier harmonics used in the expansion of the cross section in Eqs. 8–10 and in the numerators appearing in Eqs. 26, 28, and 31:

$$\mathcal{A}_{\mathrm{L}\overleftarrow{\Rightarrow}}(e_\ell = +1, P_{zz}, \phi) = \frac{K}{\mathrm{d}\sigma_{\mathrm{U}\overleftarrow{\Rightarrow}}(e_\ell = +1, P_{zz}, \phi)}$$
$$\times \left\{ K_{\mathrm{DVCS}} \Big[s^{\mathrm{DVCS}}_{1,\mathrm{unp}} \sin\phi + \frac{1}{2} P_{zz}\, (s^{\mathrm{DVCS}}_{1,\mathrm{unp}} - s^{\mathrm{DVCS}}_{1,\mathrm{LLP}}) \sin\phi \Big] \right.$$
$$\left. - \frac{K_{\mathrm{I}}}{\mathcal{P}_1(\phi)\mathcal{P}_2(\phi)} \Big[\sum_{n=1}^{2} s^{\mathrm{I}}_{n,\mathrm{unp}} \sin(n\phi) + \frac{1}{2} P_{zz} \sum_{n=1}^{2} (s^{\mathrm{I}}_{n,\mathrm{unp}} - s^{\mathrm{I}}_{n,\mathrm{LLP}}) \sin(n\phi) \Big] \right\} \tag{26}$$
$$\simeq \sum_{n=1}^{2} A^{\sin(n\phi)}_{\mathrm{L}\overleftarrow{\Rightarrow}}(e_\ell = +1, P_{zz}) \sin(n\phi)\,, \tag{27}$$

$$\mathcal{A}_{\mathrm{UL}}(e_\ell = +1, P_{zz}, \phi) = \frac{K}{\mathrm{d}\sigma_{\mathrm{U}\overleftarrow{\Rightarrow}}(e_\ell = +1, P_{zz}, \phi)}$$
$$\times \left\{ K_{\mathrm{DVCS}} \sum_{n=1}^{2} s^{\mathrm{DVCS}}_{n,\mathrm{LP}} \sin(n\phi) - \frac{K_{\mathrm{I}}}{\mathcal{P}_1(\phi)\mathcal{P}_2(\phi)} \sum_{n=1}^{3} s^{\mathrm{I}}_{n,\mathrm{LP}} \sin(n\phi) \right\} \tag{28}$$
$$\simeq \sum_{n=1}^{3} A^{\sin(n\phi)}_{\mathrm{UL}}(e_\ell = +1, P_{zz}) \sin(n\phi)\,, \tag{29}$$

$$\mathcal{A}_{\mathrm{LL}}(e_\ell = +1, P_{zz}, \phi) \equiv \frac{1}{4\,\mathrm{d}\sigma_{\mathrm{U}\overleftarrow{\Rightarrow}}(e_\ell = +1, P_{zz}, \phi)}$$
$$\times \left\{ \Big[\mathrm{d}\sigma^{\overrightarrow{\Rightarrow}+}(P_{zz}, \phi) + \mathrm{d}\sigma^{\overleftarrow{\Leftarrow}+}(P_{zz}, \phi) \Big] - \Big[\mathrm{d}\sigma^{\overleftarrow{\Rightarrow}+}(P_{zz}, \phi) + \mathrm{d}\sigma^{\overrightarrow{\Leftarrow}+}(P_{zz}, \phi) \Big] \right\} \tag{30}$$
$$= \frac{K}{\mathrm{d}\sigma_{\mathrm{U}\overleftarrow{\Rightarrow}}(e_\ell = +1, P_{zz}, \phi)}$$
$$\times \left\{ \frac{K_{\mathrm{BH}}}{\mathcal{P}_1(\phi)\mathcal{P}_2(\phi)} \sum_{n=0}^{1} c^{\mathrm{BH}}_{n,\mathrm{LP}} \cos(n\phi) + K_{\mathrm{DVCS}} \sum_{n=0}^{1} c^{\mathrm{DVCS}}_{n,\mathrm{LP}} \cos(n\phi) \right.$$
$$\left. - \frac{K_{\mathrm{I}}}{\mathcal{P}_1(\phi)\mathcal{P}_2(\phi)} \sum_{n=0}^{2} c^{\mathrm{I}}_{n,\mathrm{LP}} \cos(n\phi) \right\} \tag{31}$$
$$\simeq \sum_{n=0}^{2} A^{\cos(n\phi)}_{\mathrm{LL}}(e_\ell = +1, P_{zz}) \cos(n\phi)\,. \tag{32}$$

The approximation in Eqs. 27, 29, and 32 is due to the truncation of terms in the Fourier series arising from the azimuthal dependences in the common denominator and the lepton propagators of Eqs. 26, 28, and 31. The Fourier coefficients of the expansion of the asymmetries are hereafter called asymmetry amplitudes. Although these asymmetry

amplitudes differ from the coefficients appearing in Eqs. 8–10 and Eqs. 26, 28, and 31, they may provide similar information in the comparison of model predictions with data.

5.2. *Single-beam-helicity formalism*

In order to extract more information on various combinations of Fourier coefficients in Eqs. 8–10, it is possible to use data collected with negative polarization of the e^- beam in conjunction with the subset of positron data with the same sign of the beam polarization. In this case, another set of Fourier coefficients of the *single-beam-helicity* asymmetries $\mathcal{A}_{\overset{\mathrm{C}}{\leftarrow}\overset{\Leftarrow}{\Rightarrow}}(P_\ell, P_{zz}, \phi)$, $\mathcal{A}_{\overset{0}{\leftarrow}\mathrm{L}}(P_\ell, P_{zz}, \phi)$ and $\mathcal{A}_{\overset{\mathrm{C}}{\leftarrow}\mathrm{L}}(P_\ell, P_{zz}, \phi)$ can be simultaneously extracted, where the subscript $\overset{\mathrm{C}}{\leftarrow}\overset{\Leftarrow}{\Rightarrow}$ indicates the charge asymmetry for a lepton beam with negative polarization on a longitudinally polarized deuterium target with vanishing net vector polarization. The subscript $\overset{0}{\leftarrow}\mathrm{L}$ indicates the asymmetry with respect to longitudinal vector target polarization for a charge-averaged lepton beam again with negative beam polarization. Similarly, the subscript $\overset{\mathrm{C}}{\leftarrow}\mathrm{L}$ indicates the double asymmetry with respect to lepton charge and longitudinal vector target polarization.

The azimuthal distribution in the expectation value of the yield in this case can be written as

$$\begin{aligned}
\mathrm{d}\langle\mathcal{N}\rangle(e_\ell, P_\ell, P_z, P_{zz}, \phi) &= \mathcal{L}\,(e_\ell, P_\ell, P_z, P_{zz})\,\eta(\phi)\,\mathrm{d}\sigma_{\overset{0}{\leftarrow}\overset{\Leftarrow}{\Rightarrow}}(P_\ell, P_{zz}, \phi) \\
&\times \left[1 + e_\ell \mathcal{A}_{\overset{\mathrm{C}}{\leftarrow}\overset{\Leftarrow}{\Rightarrow}}(P_\ell, P_{zz}, \phi) + P_z \mathcal{A}_{\overset{0}{\leftarrow}\mathrm{L}}(P_\ell, P_{zz}, \phi) + e_\ell P_z \mathcal{A}_{\overset{\mathrm{C}}{\leftarrow}\mathrm{L}}(P_\ell, P_{zz}, \phi)\right]. \quad (33)
\end{aligned}$$

Here, the cross section $\mathrm{d}\sigma_{\overset{0}{\leftarrow}\overset{\Leftarrow}{\Rightarrow}}(P_\ell, P_{zz}, \phi)$ for production of real photons by a charge-averaged polarized lepton beam on a tensor-polarized deuterium target with vanishing vector polarization is defined as

$$\begin{aligned}
\mathrm{d}\sigma_{\overset{0}{\leftarrow}\overset{\Leftarrow}{\Rightarrow}}(P_\ell, P_{zz}, \phi) &\equiv \frac{1}{4}\Big[\mathrm{d}\sigma^{\overset{\leftarrow}{\Rightarrow}+}(P_\ell, P_{zz}, \phi) + \mathrm{d}\sigma^{\overset{\leftarrow}{\Leftarrow}+}(P_\ell, P_{zz}, \phi) \\
&\quad + \mathrm{d}\sigma^{\overset{\leftarrow}{\Rightarrow}-}(P_\ell, P_{zz}, \phi) + \mathrm{d}\sigma^{\overset{\leftarrow}{\Leftarrow}-}(P_\ell, P_{zz}, \phi)\Big] \quad (34) \\
&= K\Bigg\{\frac{K_{\mathrm{BH}}}{\mathcal{P}_1(\phi)\mathcal{P}_2(\phi)}\Bigg[\sum_{n=0}^{2} c_{n,\mathrm{unp}}^{\mathrm{BH}}\cos(n\phi) + \frac{1}{2}P_{zz}\sum_{n=0}^{2}(c_{n,\mathrm{unp}}^{\mathrm{BH}} - c_{n,\mathrm{LLP}}^{\mathrm{BH}})\cos(n\phi)\Bigg] \\
&+ K_{\mathrm{DVCS}}\Bigg[\sum_{n=0}^{2} c_{n,\mathrm{unp}}^{\mathrm{DVCS}}\cos(n\phi) + P_\ell\sum_{n=1}^{2} s_{n,\mathrm{unp}}^{\mathrm{DVCS}}\sin(n\phi) \\
&+ \frac{1}{2}P_{zz}\Bigg(\sum_{n=0}^{2}(c_{n,\mathrm{unp}}^{\mathrm{DVCS}} - c_{n,\mathrm{LLP}}^{\mathrm{DVCS}})\cos(n\phi) + P_\ell\sum_{n=1}^{2}(s_{n,\mathrm{unp}}^{\mathrm{DVCS}} - s_{n,\mathrm{LLP}}^{\mathrm{DVCS}})\sin(n\phi)\Bigg)\Bigg]\Bigg\}. \quad (35)
\end{aligned}$$

Then the single-beam-helicity asymmetries appearing in Eq. 33 are expressed as

$$\mathcal{A}_{\overset{\mathrm{C}}{\leftarrow}\overset{\Leftarrow}{\Rightarrow}}(P_\ell,P_{zz},\phi) \equiv \frac{1}{4\,\mathrm{d}\sigma_{\overset{0}{\leftarrow}\overset{\Leftarrow}{\Rightarrow}}(P_\ell,P_{zz},\phi)}$$
$$\times\left\{\left[\mathrm{d}\sigma^{\overset{\leftarrow}{\Rightarrow}+}(P_\ell,P_{zz},\phi)+\mathrm{d}\sigma^{\overset{\leftarrow}{\Leftarrow}+}(P_\ell,-P_z,P_{zz},\phi)\right]\right.$$
$$\left.-\left[\mathrm{d}\sigma^{\overset{\leftarrow}{\Rightarrow}-}(P_\ell,P_{zz},\phi)+\mathrm{d}\sigma^{\overset{\leftarrow}{\Leftarrow}-}(P_\ell,P_{zz},\phi)\right]\right\} \tag{36}$$
$$= \frac{K}{\mathrm{d}\sigma_{\overset{0}{\leftarrow}\overset{\Leftarrow}{\Rightarrow}}(P_\ell,P_{zz},\phi)}$$
$$\times\left\{-\frac{K_{\mathrm{I}}}{\mathcal{P}_1(\phi)\mathcal{P}_2(\phi)}\left[\sum_{n=0}^{3}c^{\mathrm{I}}_{n,\mathrm{unp}}\cos(n\phi)+P_\ell\sum_{n=1}^{2}s^{\mathrm{I}}_{n,\mathrm{unp}}\sin(n\phi)\right.\right.$$
$$\left.\left.+\frac{1}{2}P_{zz}\left(\sum_{n=0}^{3}(c^{\mathrm{I}}_{n,\mathrm{unp}}-c^{\mathrm{I}}_{n,\mathrm{LLP}})\cos(n\phi)+P_\ell\sum_{n=1}^{2}(s^{\mathrm{I}}_{n,\mathrm{unp}}-s^{\mathrm{I}}_{n,\mathrm{LLP}})\sin(n\phi)\right)\right]\right\} \tag{37}$$
$$\simeq \sum_{n=0}^{3}A^{\cos(n\phi)}_{\overset{\mathrm{C}}{\leftarrow}\overset{\Leftarrow}{\Rightarrow}}(P_{zz})\cos(n\phi)+P_\ell\sum_{n=1}^{2}A^{\sin(n\phi)}_{\overset{\mathrm{C}}{\leftarrow}\overset{\Leftarrow}{\Rightarrow}}(P_{zz})\sin(n\phi)\,, \tag{38}$$

$$\mathcal{A}_{\overset{0}{\leftarrow}\mathrm{L}}(P_\ell,P_{zz},\phi) \equiv \frac{1}{4\,\mathrm{d}\sigma_{\overset{0}{\leftarrow}\overset{\Leftarrow}{\Rightarrow}}(P_\ell,P_{zz},\phi)}$$
$$\times\left\{\left[\mathrm{d}\sigma^{\overset{\leftarrow}{\Rightarrow}+}(P_\ell,P_{zz},\phi)+\mathrm{d}\sigma^{\overset{\leftarrow}{\Rightarrow}-}(P_\ell,P_{zz},\phi)\right]\right.$$
$$\left.-\left[\mathrm{d}\sigma^{\overset{\leftarrow}{\Leftarrow}+}(P_\ell,P_{zz},\phi)+\mathrm{d}\sigma^{\overset{\leftarrow}{\Leftarrow}-}(P_\ell,P_{zz},\phi)\right]\right\} \tag{39}$$
$$= \frac{K}{\mathrm{d}\sigma_{\overset{0}{\leftarrow}\overset{\Leftarrow}{\Rightarrow}}(P_\ell,P_{zz},\phi)}$$
$$\times\left\{\frac{K_{\mathrm{BH}}}{\mathcal{P}_1(\phi)\mathcal{P}_2(\phi)}\left[P_\ell\sum_{n=0}^{1}c^{\mathrm{BH}}_{n,\mathrm{LP}}\cos(n\phi)\right]\right.$$
$$\left.+K_{\mathrm{DVCS}}\left[P_\ell\sum_{n=0}^{1}c^{\mathrm{DVCS}}_{n,\mathrm{LP}}\cos(n\phi)+\sum_{n=1}^{2}s^{\mathrm{DVCS}}_{n,\mathrm{LP}}\sin(n\phi)\right]\right\} \tag{40}$$
$$\simeq P_\ell\sum_{n=0}^{1}A^{\cos(n\phi)}_{\overset{0}{\leftarrow}\mathrm{L}}(P_{zz})\cos(n\phi)+\sum_{n=1}^{2}A^{\sin(n\phi)}_{\overset{0}{\leftarrow}\mathrm{L}}(P_{zz})\sin(n\phi)\,, \tag{41}$$

$$\mathcal{A}_{\substack{\mathrm{C}\\ \leftarrow\mathrm{L}}}(P_\ell, P_{zz}, \phi) \equiv \frac{1}{4\,\mathrm{d}\sigma_{\substack{0\\ \leftarrow\Rightarrow}}(P_\ell, P_{zz}, \phi)}$$
$$\times \left\{ \left[\mathrm{d}\sigma^{\substack{\leftarrow\\ \Rightarrow}+}(P_\ell, P_{zz}, \phi) + \mathrm{d}\sigma^{\substack{\leftarrow\\ \Leftarrow}-}(P_\ell, P_{zz}, \phi) \right] \right.$$
$$\left. - \left[\mathrm{d}\sigma^{\substack{\leftarrow\\ \Leftarrow}+}(P_\ell, P_{zz}, \phi) + \mathrm{d}\sigma^{\substack{\leftarrow\\ \Rightarrow}-}(P_\ell, P_{zz}, \phi) \right] \right\} \tag{42}$$
$$= \frac{K}{\mathrm{d}\sigma_{\substack{0\\ \leftarrow\Rightarrow}}(P_\ell, P_{zz}, \phi)}$$
$$\times \left\{ - \frac{K_\mathrm{I}}{\mathcal{P}_1(\phi)\mathcal{P}_2(\phi)} \left[P_\ell \sum_{n=0}^{2} c^\mathrm{I}_{n,\mathrm{LP}} \cos(n\phi) + \sum_{n=1}^{3} s^\mathrm{I}_{n,\mathrm{LP}} \sin(n\phi) \right] \right\} \tag{43}$$
$$\simeq P_\ell \sum_{n=0}^{2} A^{\cos(n\phi)}_{\substack{\mathrm{C}\\ \leftarrow\mathrm{L}}}(P_{zz}) \cos(n\phi) + \sum_{n=1}^{3} A^{\sin(n\phi)}_{\substack{\mathrm{C}\\ \leftarrow\mathrm{L}}}(P_{zz}) \sin(n\phi)\,. \tag{44}$$

All the asymmetries defined in this paper are summarized in Table 3.

Table 3
Extracted beam-helicity, beam-charge and target-spin asymmetries on a polarized deuterium target. The symbol ■ marks which data taken under certain experimental conditions (beam polarization, beam charge and target polarization state) are available for the construction of the respective asymmetry. The − or + indicates the sign with which the corresponding yield enters the numerator of the asymmetry. For the case that the target is populated with deuterons in the state $\Lambda = \pm 1$, the ideal target polarizations are $P_z = \pm 1$ and $P_{zz} = 1$, while for the case $\Lambda = 0$, $P_z = 0$ and $P_{zz} = -2$. The sensitivity of coherent scattering to the corresponding Compton form factors or BH amplitude is indicated.

		Lepton charge		Target population (deuterons)					Beam helicity			
				$\Lambda=+1$		$\Lambda=-1$		$\Lambda=0$	$\lambda=+1$		$\lambda=-1$	Coherent
		$+1$	-1	$\Rightarrow$		$\Leftarrow$		0	$\rightarrow$		$\leftarrow$	sensitivity
Single-charge	$\mathcal{A}_{\mathrm{L}\substack{\Leftarrow\\ \Rightarrow}}$	■		■	+	■			■	−	■	$\Im\mathrm{m}(\mathcal{H}_1, \mathcal{H}_5)$
	$\mathcal{A}_{\mathrm{UL}}$	■		■	−	■			■	+	■	$\Im\mathrm{m}(\widetilde{\mathcal{H}}_1)$
	$\mathcal{A}_{\mathrm{LL}}$	■		■	−	■			■	−	■	(BH)
	$\mathcal{A}_{\mathrm{L}zz}$	■		■	+	■	−	■	■	−	■	$\Im\mathrm{m}(\mathcal{H}_5)$
Single-helicity	$\mathcal{A}_{\substack{\mathrm{C}\\ \leftarrow\Leftrightarrow}}$	■	− ■	■	+	■					■	$\Im\mathrm{m}/\Re\mathrm{e}(\mathcal{H}_1, \mathcal{H}_5)$
	$\mathcal{A}_{\substack{0\\ \leftarrow\mathrm{L}}}$	■	+ ■	■	−	■					■	(BH)
	$\mathcal{A}_{\substack{\mathrm{C}\\ \leftarrow\mathrm{L}}}$	■	− ■	■	−	■					■	$\Im\mathrm{m}/\Re\mathrm{e}(\widetilde{\mathcal{H}}_1)$

6. Background corrections and systematic uncertainties

The asymmetry amplitudes are corrected for background contributions, mainly decays to two photons of semi-inclusive neutral mesons, using the method described in detail in Ref. [42]. The average contribution from semi-inclusive background is 4.6%. The contribution of exclusive pions is neglected, as it is found to be less than 0.7% in each kinematic bin, supported by studies of HERMES data [43]. After applying this correction, the re-

sulting asymmetry amplitudes are expected to originate from coherent and incoherent photon production, the latter possibly including nucleon excitation.

The dominant contributions to the total systematic uncertainty are the effects of the limited spectrometer acceptance and from the finite bin widths used for the final presentation of the results. The latter originates from the difference of the amplitudes integrated over one bin in all kinematic variables, compared to the asymmetry amplitudes calculated at the average values of the kinematic variables. The combined contribution to the systematic uncertainty from limited spectrometer acceptance, finite bin width, and the alignment of the spectrometer elements with respect to the beam is determined from a Monte Carlo simulation using a convenient parameterization [44] of the VGG model [45] (see details in Ref. [27]). Five GPD model variants are considered, including only incoherent processes on the proton and neutron. In each kinematic bin, the resulting systematic uncertainty is defined as the root-mean-square average of the five differences between the asymmetry amplitude extracted from the Monte Carlo data and the corresponding model predictions calculated analytically at the mean kinematic values of that bin. In the case of the single-charge beam-helicity asymmetry, all five models overpredict the magnitudes of the $\sin\phi$ harmonics by about a factor of two, leading to a probable overestimate of this contribution to the uncertainties. The other source of uncertainty is associated with the background correction. For asymmetries involving target vector polarization, no systematic uncertainty due to luminosity is assigned. This is legitimate because the luminosity does not depend on the target polarization, the target polarization flips rapidly compared to changes in luminosity, and beam polarization dependent weights are assigned to each event in the extraction. There is an additional overall scale uncertainty arising from the uncertainty in the measurement of the beam and/or target polarizations. Not included is any contribution due to additional QED vertices, as for the case of polarized target and polarized beam the most significant of these has been estimated to be negligible [46]. The total systematic uncertainty in a kinematic bin is determined by adding quadratically all contributions to the systematic uncertainty for that bin.

7. Results

7.1. *Single- and double-spin asymmetries*

The results for the Fourier amplitudes of the single-charge asymmetries $\mathcal{A}_{\mathrm{L}\overleftrightarrow{}}(e_\ell = +1, P_{zz}, \phi)$, $\mathcal{A}_{\mathrm{UL}}(e_\ell = +1, P_{zz}, \phi)$ and $\mathcal{A}_{\mathrm{LL}}(e_\ell = +1, P_{zz}, \phi)$ are presented in Figs. 1–3 as a function of $-t$, x_N, or Q^2 and are also given in Table 5. While the variable x_D would be the appropriate choice to present experimental results for pure coherent scattering, the nucleonic Bjorken variable x_N is the practical choice in this case where incoherent scattering dominates over most of the kinematic range. The 'overall' results in the left columns correspond to the entire HERMES kinematic acceptance. Figure 1 shows the amplitudes $A_{\mathrm{L}\overleftrightarrow{}}^{\sin(n\phi)}$ related to beam helicity only, while Figs. 2 and 3 show the amplitudes $A_{\mathrm{UL}}^{\sin(n\phi)}$, which relate to target vector polarization only, and the amplitudes $A_{\mathrm{LL}}^{\cos(n\phi)}$, which relate to the product of beam helicity and target vector polarization. Table 4 and Fig. 4 show in each kinematic bin the estimated fractional contributions to the yield from the coherent process and from processes leading to baryonic resonant

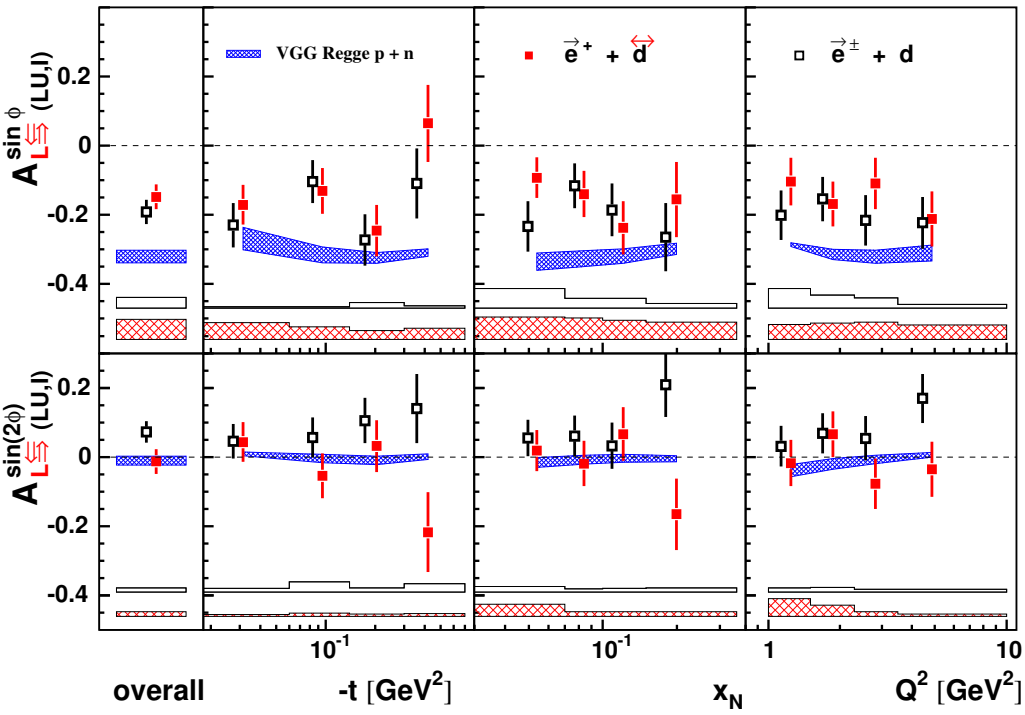

Fig. 1. Results from the present work (red filled squares) representing single-charge beam-helicity asymmetry amplitudes $A_{\mathrm{L}\overleftrightarrow{S}}^{\sin(n\phi)}$ describing the dependence of the sum of squared DVCS and interference terms on the beam helicity, for a tensor polarization of $P_{zz} = 0.827$ (indicated by the symbol $\leftrightarrow$). The black open squares represent charge-difference amplitudes $A_{\mathrm{LU,I}}^{\sin(n\phi)}$ from only the interference term, extracted from unpolarized deuterium data [27]. The error bars represent the statistical uncertainties, while the coarsely hatched (open) bands represent the systematic uncertainties of the filled (open) squares. There is an additional overall 1.9% (2.4%) scale uncertainty arising from the uncertainty in the measurement of the beam polarization in the case of polarized (unpolarized) deuterium data. The points for unpolarized deuterium data are slightly shifted to the left for better visibility. The finely hatched band shows the results of theoretical calculations for the combination of incoherent scattering on proton and neutron, using variants of the VGG double-distribution model [45,48] with a Regge ansatz for modeling the t dependence of GPDs [49].

final states. They are obtained from a Monte Carlo simulation using an exclusive-photon generator described in Ref. [27].

The values for the $\sin\phi$ amplitude of the asymmetry $\mathcal{A}_{\mathrm{L}\overleftrightarrow{S}}$ in Fig. 1 are found to be significantly negative, while the $\sin(2\phi)$ amplitude is found to be consistent with zero. Figure 1 also presents for comparison the amplitudes of the charge-difference asymmetry $\mathcal{A}_{\mathrm{LU}}^{\mathrm{I}}$ extracted from a previous measurement on unpolarized deuterons [27]. Under the same approximations as those leading to Eq. 13, $\mathcal{A}_{\mathrm{L}\overleftrightarrow{S}}$ is expected to differ from $\mathcal{A}_{\mathrm{LU}}^{\mathrm{I}}$ (only if $P_{zz} \neq 0$) due only to a term involving the CFF $\mathcal{H}_5$. Figure 1 shows that these two asymmetries are found to be consistent in most kinematic regions, except possibly for the last $-t$ or x_N bin in the case of $\sin(2\phi)$. (The overall results differ by only 1.7 standard deviations in the total experimental uncertainties. [7]) The consistency in the first

[7] Here and hereafter we neglect any possible correlations arising from common treatments of different

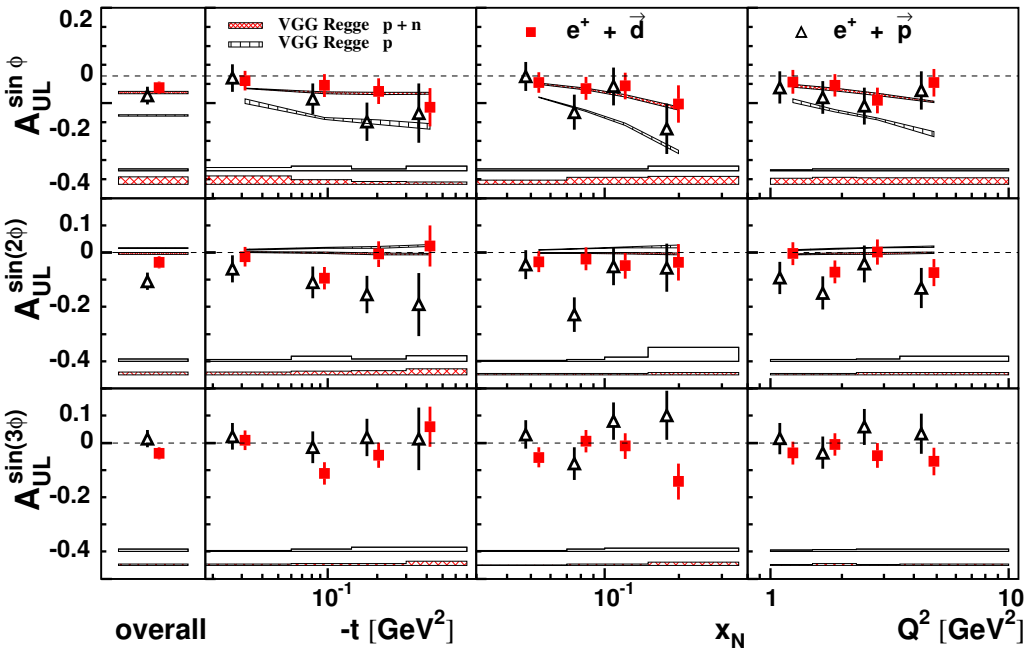

Fig. 2. Single-charge target-spin asymmetry amplitudes describing the dependence of the sum of squared DVCS and interference terms on the target vector polarization, for a tensor polarization of $P_{zz} = 0.827$. The squares represent the results from the present work. The triangles denote the corresponding amplitudes extracted from longitudinally polarized hydrogen data [24]. The error bars (bands) represent the statistical (systematic) uncertainties. The finely hatched bands have the same meaning as in Fig. 1. There is an additional overall 4.0% (4.2%) scale uncertainty arising from the uncertainty in the measurement of the target polarization in the case of deuterium (hydrogen). The points for hydrogen are slightly shifted to the left for better visibility.

$-t$ bin, where the contribution from coherent scattering is significant, suggests that there is no distinctive contribution from $\mathcal{H}_5$, as was observed in the case of the corresponding forward limit [20,21].

In the first $-t$ bin, the asymmetry amplitude $A^{\sin\phi}_{\mathrm{L}\overleftrightarrow{\Rightarrow},\mathrm{coh}}$ for pure coherent scattering on a polarized deuterium target was estimated from the measured asymmetry by correcting for the incoherent contributions of the proton and neutron and their resonances (see Ref. [27]). This correction is based on the assumption that for the incoherent contribution of the proton, $A^{\sin\phi}_{\mathrm{L}\overleftrightarrow{\Rightarrow}}(P_{zz} = 0.827) \approx A^{\sin\phi}_{\mathrm{LU,I}}$ where the latter was measured on a hydrogen target [26]. The fractional contributions and the asymmetry for incoherent scattering from the neutron was taken from the Monte Carlo calculation described in section 6, with uncertainties equal to their magnitude. The result for the asymmetry amplitude $A^{\sin\phi}_{\mathrm{L}\overleftrightarrow{\Rightarrow},\mathrm{coh}}(P_{zz} = 0.827)$ is estimated to be $-0.12 \pm 0.17(\mathrm{stat.}) \pm 0.14(\mathrm{syst.}) \pm 0.02(\mathrm{model})$, where the systematic uncertainty is propagated from only the corresponding experimental uncertainties. Within the uncertainties there is no evidence of a difference between this value and the value for the asymmetry amplitude $A^{\sin\phi}_{\mathrm{LU,I,coh}} = -0.29 \pm 0.18(\mathrm{stat.}) \pm 0.03(\mathrm{syst.})$ previously estimated for coherent scattering on an unpolarized deuterium

data sets.

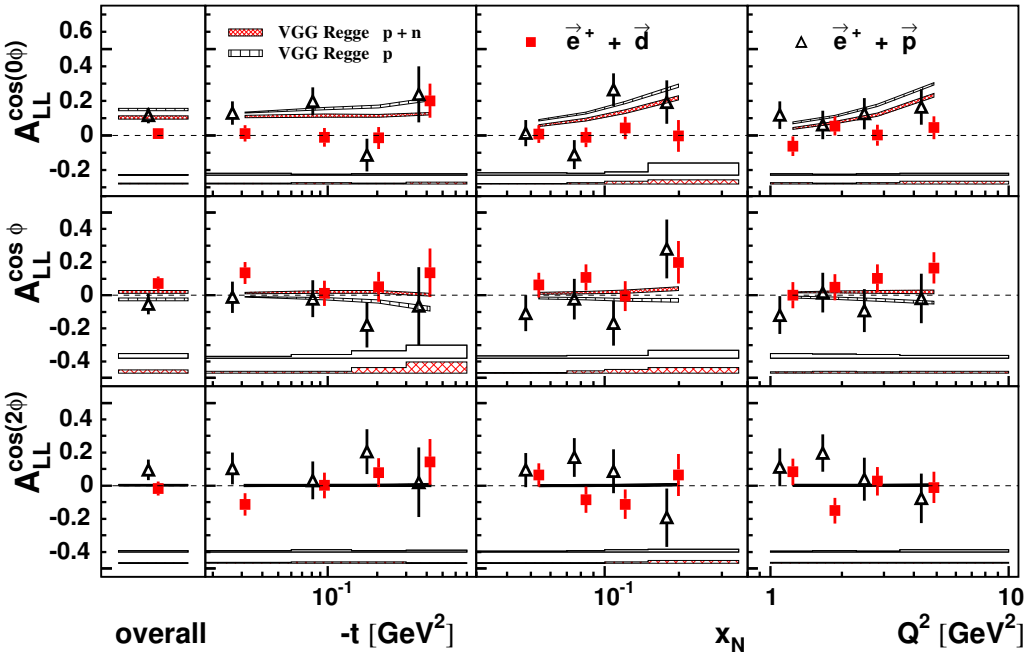

Fig. 3. Single-charge double-spin asymmetry amplitudes describing the dependence of the sum of Bethe-Heitler, squared DVCS and interference terms on the product of the beam helicity and target vector polarization, for a tensor polarization of $P_{zz} = 0.827$. The plotted symbols and bands have the same meaning as in Fig. 2. There is an additional overall 4.4% (5.3%) scale uncertainty arising from the uncertainties in the measurement of the beam and target polarizations in the case of deuterium (hydrogen) data.

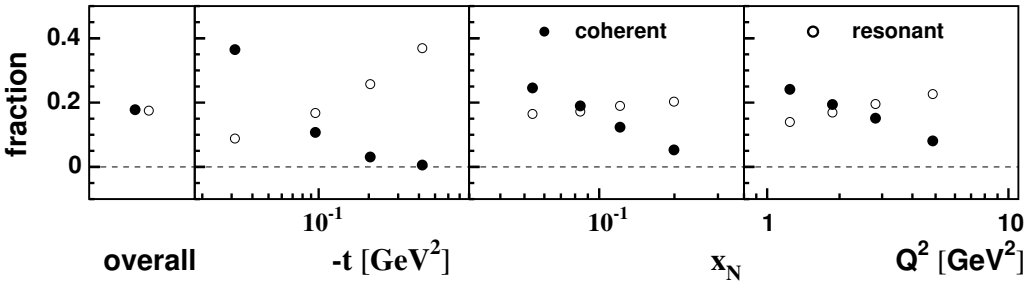

Fig. 4. Simulated yield fractions of coherent and resonant production

target, using a disjoint HERMES data set for an unpolarized deuterium target [27], but using the same data set for a hydrogen target.

The extracted values for the $\sin\phi$ and $\sin(2\phi)$ amplitudes of the single-charge asymmetry $\mathcal{A}_{\rm UL}$ measured on a longitudinally polarized deuterium target are shown in Fig. 2. The 'overall' values are slightly negative by less than 1.5 standard deviations of the total experimental uncertainty. For coherent scattering on the deuteron, the amplitude $A_{\rm UL}^{\sin\phi}$ is sensitive to the imaginary part of a combination of deuteron CFFs $\widetilde{\mathcal{H}}_1$, $\mathcal{H}_1$ and $\mathcal{H}_5$ weighted with the elastic form factors of the deuteron G_1 and G_2 (see Eq. 21). In particular, for the first $-t$ bin where $\langle x_D\rangle = 0.04$, G_1 is about 30 times larger than $\frac{x_D}{2}G_2$. Thus

Table 4
Simulated fractional contributions of coherent and resonant processes on a deuteron, in each kinematic bin.

Kinematic bin		$\langle -t \rangle$ [GeV^2]	$\langle x_N \rangle$	$\langle Q^2 \rangle$ [GeV^2]	Coherent	Resonant
Overall		0.13	0.10	2.5	0.177	0.177
$-t$[GeV^2]	0.00 - 0.06	0.03	0.08	1.9	0.364	0.088
	0.06 - 0.14	0.10	0.10	2.5	0.107	0.168
	0.14 - 0.30	0.20	0.11	2.9	0.030	0.257
	0.30 - 0.70	0.42	0.12	3.5	0.006	0.369
x_N	0.03 - 0.07	0.11	0.05	1.4	0.246	0.164
	0.07 - 0.10	0.11	0.08	2.1	0.189	0.172
	0.10 - 0.15	0.14	0.12	3.1	0.123	0.189
	0.15 - 0.35	0.20	0.20	5.0	0.053	0.202
Q^2[GeV^2]	1.0 - 1.5	0.09	0.06	1.2	0.241	0.139
	1.5 - 2.3	0.11	0.08	1.9	0.194	0.169
	2.3 - 3.5	0.14	0.11	2.8	0.151	0.196
	3.5 - 10.0	0.20	0.17	4.9	0.080	0.226

the CFF $\widetilde{\mathcal{H}}_1$ may influence the resulting $A_{\rm UL}^{\sin\phi}$ amplitude in the first $-t$ bin where the coherent process contributes approximately 40%. For comparison, the same amplitudes measured on a longitudinally polarized hydrogen target [24] are also shown in Fig. 2. The $\sin\phi$ amplitude shows consistency between deuterium and hydrogen data both for the 'overall' result and the kinematic projections on $-t$, x_N, and Q^2. In this comparison, no account was taken of the 7.5% depolarization of nucleons in the deuteron due to the 5% admixture of the D-state [47]. The 'overall' results on the $\sin(2\phi)$ amplitude differ between the two targets by 1.5 standard deviations of the total experimental uncertainties, mainly due to the region of large $-t$, but in only one x_N bin. The 'overall' result on the asymmetry amplitude $A_{\rm UL}^{\sin(3\phi)}$ is slightly negative by less than 1.7 standard deviations of the total experimental uncertainty. The $\sin(3\phi)$ amplitude shows consistency between deuterium and hydrogen data, accounting for the total experimental uncertainties of the corresponding measurements, except possibly for the highest x_N bin.

The $A_{\rm LL}^{\cos(n\phi)}$ amplitudes of the single-charge double-spin asymmetry measured using longitudinally polarized deuteron data and presented in Fig. 3 are found to be compatible with zero, although the $A_{\rm LL}^{\cos\phi}$ amplitude is positive by 1.6 standard deviations of the total experimental uncertainty. Within the uncertainties, these asymmetry amplitudes do not show significant differences from those measured on a longitudinally polarized hydrogen target [24], except possibly for the overall result for the amplitude $A_{\rm LL}^{\cos(0\phi)}$, where there is observed a discrepancy of 1.9 standard deviations in the total experimental uncertainties.

The finely hatched bands in Figs. 1–3 represent results of theoretical calculations based

on the GPD model described in Ref. [45], using the VGG computer program of Ref. [48]. The Regge ansatz for modeling the t dependence of GPDs [49] is used in these calculations. The model [45] is an implementation of the double-distribution concept [1,2] where the kernel of the double distribution contains a profile function that determines the dependence on ξ, controlled by a parameter b [50] for each quark flavor. The cross sections are calculated as the sum of the incoherent processes on the proton and neutron in each kinematic bin. (No computer program is available simulating coherent scattering on the deuteron.) The width of the theoretical bands in Figs. 1–3 corresponds to the range of values of the asymmetry amplitudes obtained by varying the profile parameters $b_{\rm val}$ and $b_{\rm sea}$ between unity and infinity. In the comparison of these predictions with experimental results, it should be noted that the effect of the D-state of the deuteron on the polarization of the nucleons inside the deuteron was not taken into account.

The model calculations predict a magnitude of the $\sin\phi$ harmonic of the single-charge beam-helicity asymmetry that exceeds that of the data by about a factor of two, a situation similar to that found in the case of a hydrogen target [26]. On the other hand the predictions are in good agreement with data for single-charge target-spin asymmetries. A large difference appears between the predictions for the $\sin\phi$ harmonic of this asymmetry on the deuteron and proton targets, arising entirely from the contributions of the neutron. The data are consistent with this difference, but lack the precision to confirm the large positive prediction of the neutron asymmetry by this model. The predictions are in good agreement with the single-charge double-spin asymmetry amplitudes, aside from the $\cos(0\phi)$ harmonic. Here the theoretical predictions for both the deuteron and proton, which are dominated by the BH contribution, are significantly positive, in agreement with the proton data, while the more precise deuteron data are consistent with zero. The small contribution of coherent scattering to the overall result, with a predicted negative asymmetry [18], is expected to slightly reduce this asymmetry amplitude for the deuteron.

7.2. *The beam-charge, charge-averaged, and beam-charge⊗target-spin asymmetries*

The results for the Fourier amplitudes of the single-beam-helicity asymmetries are presented in Figs. 5–7. More specifically, Figs. 5, 6, and 7 show the $\cos(n\phi)$ and $\sin(n\phi)$ harmonics of the asymmetry $\mathcal{A}_{\substack{\rm C\\ \leftarrow\\ \Rightarrow}}(P_\ell, P_{zz}, \phi)$, $\mathcal{A}_{\substack{0\\ \leftarrow\\ \rm L}}(P_\ell, P_{zz}, \phi)$ and $\mathcal{A}_{\substack{\rm C\\ \leftarrow\\ \rm L}}(P_\ell, P_{zz}, \phi)$, respectively (see also Tables 6–8), for $P_\ell = -0.530 \pm 0.012$ and $P_{zz} = 0.827 \pm 0.027$.

The only overall results for the asymmetry $\mathcal{A}_{\substack{\rm C\\ \leftarrow\\ \Rightarrow}}$ in Fig. 5 that are found to be significantly non-zero are the $\cos\phi$ and $\sin\phi$ amplitudes. The theoretical calculations for incoherent scattering predict that the results for the amplitudes $A_{\substack{\rm C\\ \leftarrow\\ \Rightarrow}}^{\cos(n\phi)}$ should strongly resemble those for the amplitudes $A_{\rm C}^{\cos(n\phi)}$ measured with an unpolarized beam on an unpolarized deuterium target [27]. The data confirm this resemblance, even in the first $-t$ bin where coherent scattering contributes about 40% of the yield. This is another indication that the CFF $\mathcal{H}_5$ [18], in this case its real part, makes no distinctive contribution to coherent scattering off deuterons, similar to the case of $A_{\substack{\rm L\\ \Leftrightarrows}}^{\sin\phi}$, as was noted in the discussion in Section 7.1 about the dependence of $A_{\substack{\rm L\\ \Leftrightarrows}}^{\sin\phi}$ of Eq. 13 on the imaginary part of this CFF.

The numerators of the $A_{\substack{\rm C\\ \leftarrow\\ \Rightarrow}}^{\sin(n\phi)}$ amplitudes shown in Fig. 5 differ from those of the $\sin(n\phi)$ amplitudes of the $\mathcal{A}_{\substack{\rm L\\ \Leftrightarrows}}$ asymmetry shown in Fig. 1 only by squared DVCS terms.

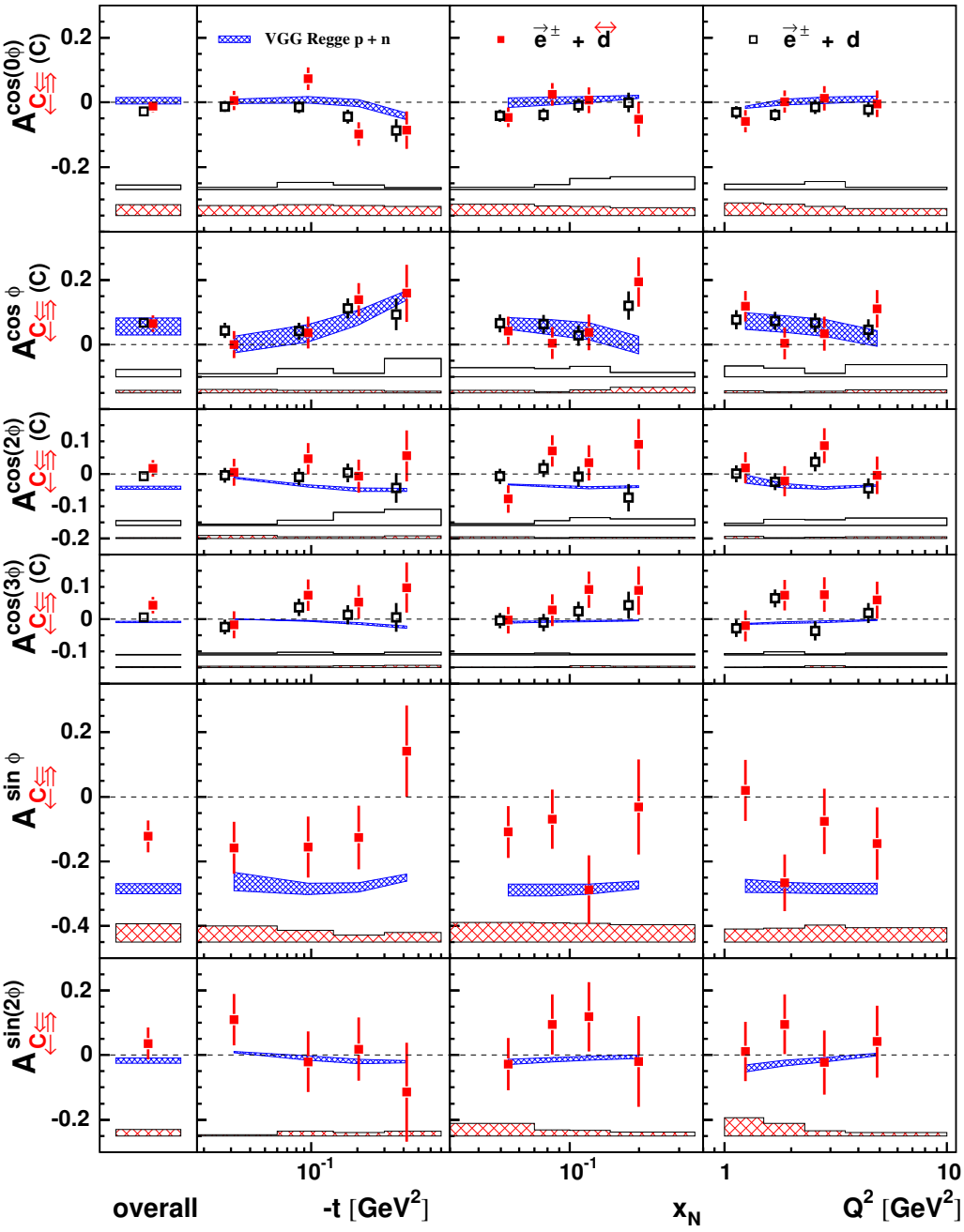

Fig. 5. Results from the present work (red filled squares) representing single-beam-helicity charge asymmetry amplitudes $A_{C\overleftrightarrows}^{\cos(n\phi)}$ and $A_{C\overleftrightarrows}^{\sin(n\phi)}$, for $P_\ell = -0.530$ and a tensor polarization of $P_{zz} = 0.827$ (indicated by the symbol $\leftrightarrow$). The black open squares are $A_{\rm C}^{\cos(n\phi)}$ amplitudes extracted from data recorded with an unpolarized beam and unpolarized deuterium target [27]. The error bars and bands and finely hatched bands have the same meaning as in Fig. 1. The points for unpolarized deuterium data are slightly shifted to the left for better visibility. There is an additional overall 2.2% scale uncertainty for the $A_{\overleftarrow{C}\rightleftarrows}^{\sin(n\phi)}$ amplitudes arising from the uncertainty in the measurement of the beam polarization.

Furthermore, the cross sections $d\sigma_{\overleftarrow{0}\,\overleftarrow{\Rightarrow}}$ and $d\sigma_{U\overleftarrow{\Rightarrow}}$ in the denominators of these two asymmetries should be similar because they are dominated by Bethe-Heitler contributions. Hence, these asymmetry amplitudes are expected to be similar, and within the statistical accuracy this is indeed found to be the case.

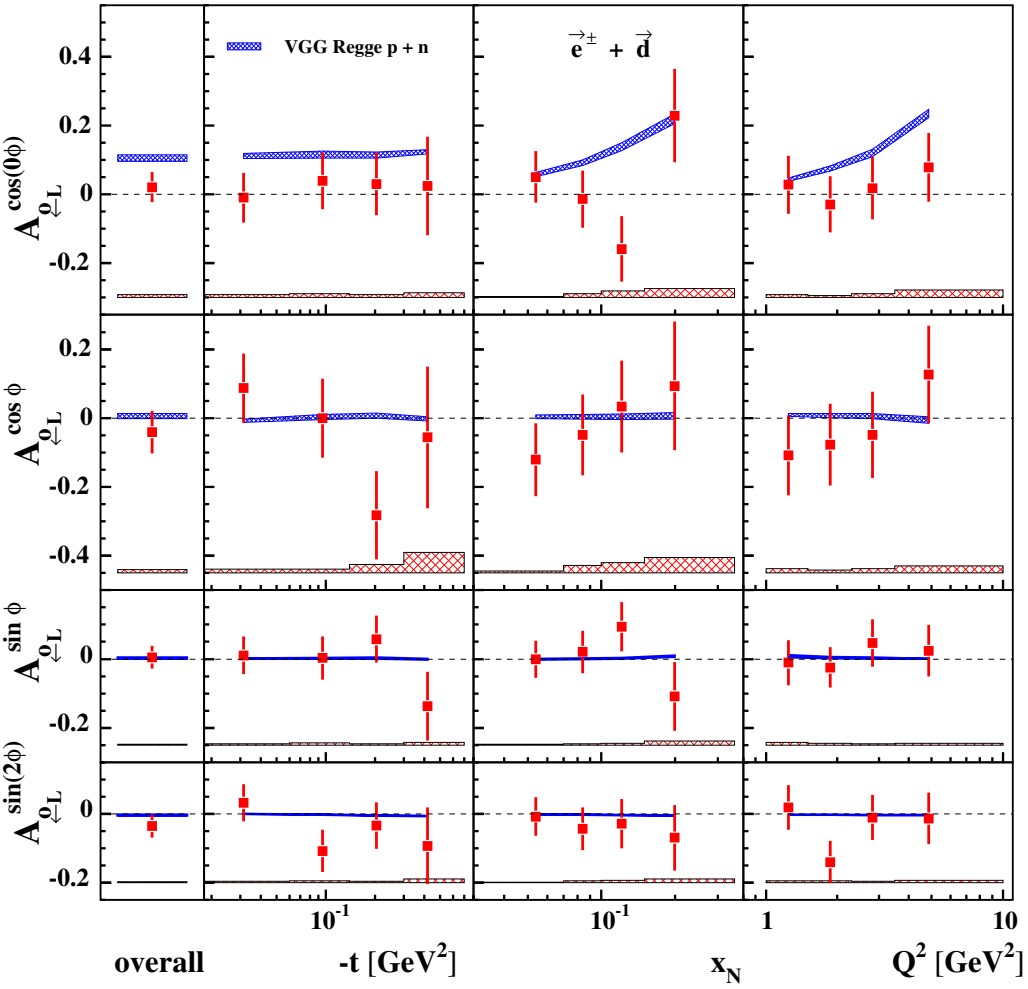

Fig. 6. Kinematic dependence of the charge-averaged single-beam-helicity target-spin asymmetry amplitudes $A_{\overleftarrow{0}_L}^{\cos(n\phi)}$ and $A_{\overleftarrow{0}_L}^{\sin(n\phi)}$, for $P_\ell = -0.530$ and a tensor polarization of $P_{zz} = 0.827$. The plotted symbols and bands have the same meaning as in Fig. 5. There is an additional overall 5.3% (5.7%) scale uncertainty for the extracted $A_{\overleftarrow{0}_L}^{\sin(n\phi)}$ $\left(A_{\overleftarrow{0}_L}^{\cos(n\phi)}\right)$ amplitudes arising from the uncertainties in the measurement of the target (beam and target) polarizations.

The $\cos(n\phi)$ amplitudes of the asymmetry $\mathcal{A}_{\overleftarrow{0}_L}$ in Fig. 6 contain a sum of BH and squared DVCS even harmonics, and relate to the longitudinal vector polarization of the target. However, even where the BH contribution dominates the numerator of the asymmetry amplitude $A_{\overleftarrow{0}_L}^{\cos(0\phi)}$ for incoherent scattering at not small $-t$, the data are

found to be consistent with zero, and differing by 1.7 standard deviations in the total experimental uncertainty from the positive prediction for the overall result. The $\sin(n\phi)$ amplitudes of the asymmetry $\mathcal{A}_{\overset{0}{\leftarrow}\mathrm{L}}$ in Fig. 6 receive contributions from the pure squared DVCS harmonics only, and are found to be consistent with zero.

Of particular interest are the $A_{\overset{\mathrm{C}}{\leftarrow}\mathrm{L}}^{\cos(n\phi)}$ and $A_{\overset{\mathrm{C}}{\leftarrow}\mathrm{L}}^{\sin(n\phi)}$ amplitudes shown in Fig. 7, which represent respectively the even and odd vector-polarization related harmonics of the interference term only, receiving no contribution from pure BH and DVCS terms. The theoretical predictions for the $\cos(n\phi)$ harmonics are negligibly small, while the data differ from zero by about two standard deviations for the first two harmonics. As expected and observed in the case of unpolarized hydrogen and deuterium targets, the $\cos(0\phi)$ and $\cos\phi$ harmonics are found to have opposite signs.

Like the asymmetry amplitude $A_{\mathrm{UL}}^{\sin(\phi)}$, in the first $-t$ bin the asymmetry amplitude $A_{\overset{\mathrm{C}}{\leftarrow}\mathrm{L}}^{\sin\phi}$ is sensitive to the imaginary part of the deuteron CFF $\widetilde{\mathcal{H}}_1$. Within their statistical accuracies, they are found to be consistent, although $A_{\mathrm{UL}}^{\sin\phi}$ receives also a contribution from the squared DVCS term (see Eq. 29). The asymmetry amplitude $A_{\overset{\mathrm{C}}{\leftarrow}\mathrm{L}}^{\cos\phi}$ is sensitive to the real part of the deuteron CFF $\widetilde{\mathcal{H}}_1$. Unlike the corresponding harmonic $A_{\mathrm{LL}}^{\cos\phi}$, it does not receive a contribution from the Bethe–Heitler term. The $\sin(n\phi)$ harmonics are found to be consistent with zero and also with the small negative prediction in the case of the $\sin\phi$ harmonic.

From the definitions of the asymmetries $\mathcal{A}_{\mathrm{UL}}$, $\mathcal{A}_{\mathrm{LL}}$, $\mathcal{A}_{\overset{0}{\leftarrow}\mathrm{L}}$ and $\mathcal{A}_{\overset{\mathrm{C}}{\leftarrow}\mathrm{L}}$ in Eqs. 19, 30, 39, and 42, and also from examination of Table 2, it can be seen that they are related. In the case of approximate equality of $\mathrm{d}\sigma_{\overset{0}{\leftarrow}\overset{\Leftarrow}{\Rightarrow}}$ and $\mathrm{d}\sigma_{\mathrm{U}\overset{\Leftarrow}{\Rightarrow}}$, the following relations hold between the asymmetry amplitudes:

$$A_{\mathrm{UL}}^{\sin(n\phi)} \simeq A_{\overset{0}{\leftarrow}\mathrm{L}}^{\sin(n\phi)} + A_{\overset{\mathrm{C}}{\leftarrow}\mathrm{L}}^{\sin(n\phi)}\,, \quad n = 1, 2\,, \tag{45}$$

$$A_{\mathrm{LL}}^{\cos(n\phi)} \simeq A_{\overset{0}{\leftarrow}\mathrm{L}}^{\cos(n\phi)} + A_{\overset{\mathrm{C}}{\leftarrow}\mathrm{L}}^{\cos(n\phi)}\,, \quad n = 0, 1\,. \tag{46}$$

For most of the kinematic points, the differences between left and right hand sides of Eqs. 45 and 46 are found below 1.2 standard deviations of the total experimental uncertainties, while for the remaining six points they are between 1.5 and 2.0. Note that here the correlations between two asymmetries from the right hand sides are taken into account.

7.3. *The beam-helicity ⊗tensor asymmetry* $\mathcal{A}_{\mathrm{Lzz}}$

The definition of the asymmetry $\mathcal{A}_{\mathrm{Lzz}}$ is given in Eq. 16. As mentioned in Section 3, for the extraction of this asymmetry, the data taken with a positron beam and with the average target tensor polarization $P_{zz} = -1.656$ are used in combination with the positron data collected on a longitudinally polarized deuterium target with $P_{zz} = 0.827$. The same maximum likelihood technique [42] unbinned in azimuthal angle ϕ was used to extract the $\mathcal{A}_{\mathrm{Lzz}}^{\sin(n\phi)}$ Fourier amplitudes. The $\mathcal{A}_{\mathrm{Lzz}}^{\sin\phi}$ amplitude is found to have the value $\mathcal{A}_{\mathrm{Lzz}}^{\sin\phi} = -0.130 \pm 0.121(stat.) \pm 0.051(syst.)$ when extracted in the entire kinematic range of the data set, while in the region $-t < 0.06\,\mathrm{GeV}^2$, where the contribution from coherent scattering on a longitudinally polarized deuteron is approximately 40%, this value is found to be $0.074 \pm 0.196(stat.) \pm 0.022(syst.)$. These results are subject

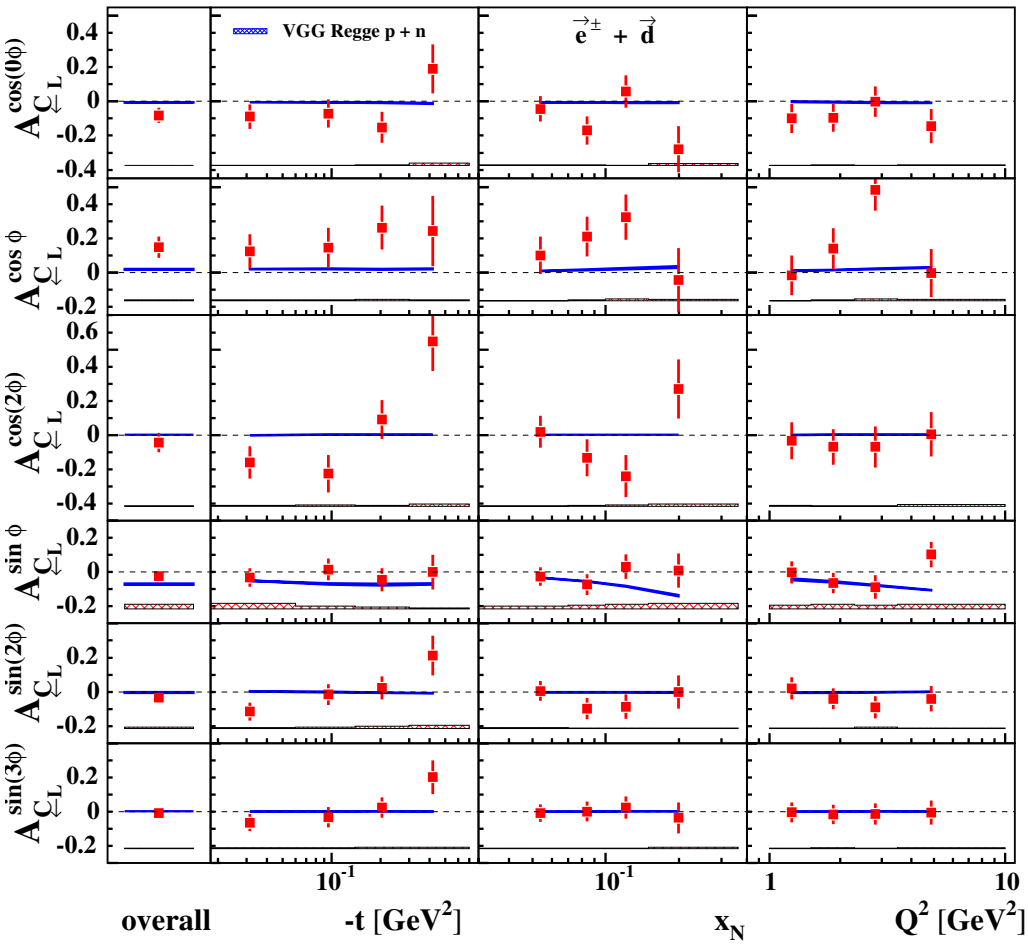

Fig. 7. Kinematic dependence of the single-beam-helicity beam-charge⊗target-spin asymmetry amplitudes $A_{C\overleftarrow{L}}^{\cos(n\phi)}$ and $A_{C\overleftarrow{L}}^{\sin(n\phi)}$, for $P_\ell = -0.530$ and a tensor polarization of $P_{zz} = 0.827$. The plotted symbols and bands have the same meaning as in Fig. 5. There is an additional overall 5.3% (5.7%) scale uncertainty for the extracted $A_{C\overleftarrow{L}}^{\sin(n\phi)}$ $\left(A_{C\overleftarrow{L}}^{\cos(n\phi)}\right)$ amplitudes arising from the uncertainties in the measurement of the target (beam and target) polarizations.

to an additional scale uncertainty of 3.8% arising from beam and target-tensor polarizations. The Fourier amplitudes related to higher twist are found to be compatible with zero within the statistical uncertainties. This 'zero' result for the beam-helicity⊗tensor asymmetry $\mathcal{A}_{\mathrm{Lzz}}$ extracted independently of the results for $\mathcal{A}_{\mathrm{LU}}^{\mathrm{I}}$ and $\mathcal{A}_{\mathrm{L}\lessgtr}$ confirms that there is no distinctive contribution from the deuteron CFF $\mathcal{H}_5$ for coherent scattering.

8. Summary

Azimuthal asymmetries with respect to target polarization alone and also combined with beam helicity and/or beam charge for hard exclusive electroproduction of real pho-

tons in deep-inelastic scattering from a longitudinally polarized deuterium target are measured for the first time. The asymmetries are attributed to the interference between the deeply virtual Compton scattering and Bethe–Heitler processes. The asymmetries are observed in the exclusive region $-(1.5)^2\,\mathrm{GeV}^2 < M_X^2 < (1.7)^2\,\mathrm{GeV}^2$ of the squared missing mass. The dependences of these asymmetries on $-t$, x_N, or Q^2 are investigated. The results include the coherent process $e\,d \to e\,d\,\gamma$ and the incoherent process $e\,d \to e\,p\,n\,\gamma$ where in addition a nucleon may be excited to a resonance. Within the total experimental uncertainties, the results of the sinusoidal (cosinusoidal) amplitudes of the asymmetry $\mathcal{A}_{\mathrm{L}\overleftrightarrows}$ ($\mathcal{A}_{\mathrm{C}\underset{\rightrightarrows}{\leftleftarrows}}$) extracted from a data set with $P_{zz} = 0.827$ (corresponding to a small population for the $\Lambda = 0$ state) resemble those for the amplitudes extracted from unpolarized deuterium data at HERMES. Therefore, no indication of effects of tensor polarization was found at small values of $-t$, in particular in the region $-t < 0.06\,\mathrm{GeV}^2$ where the coherent process contributes up to 40%. Neither the $\mathcal{A}_{\mathrm{UL}}^{\sin(n\phi)}$ nor $\mathcal{A}_{\mathrm{LL}}^{\cos(n\phi)}$ amplitudes measured on longitudinally polarized deuterons show significant differences compared with those extracted from longitudinally polarized protons, considering the total experimental uncertainties. (Statistically marginal differences are observed for $\mathcal{A}_{\mathrm{UL}}^{\sin(2\phi)}$ and $\mathcal{A}_{\mathrm{LL}}^{\cos(0\phi)}$).

The sinusoidal amplitudes of the tensor asymmetry A_{Lzz} are compatible with zero for the whole kinematic range as well as for the region $-t < 0.06\,\mathrm{GeV}^2$ within the accuracy of the measurement. This suggests that differences between the leading amplitudes of the asymmetries $\mathcal{A}_{\mathrm{LU}}^{\mathrm{I}}$ and $\mathcal{A}_{\mathrm{L}\overleftrightarrows}$ for coherent scattering from unpolarized and longitudinally polarized deuterium targets, respectively, should be small. Indeed, within the total experimental uncertainties, no difference is seen between the reconstructed values of the asymmetry amplitudes $A_{\mathrm{L}\overleftrightarrows,\mathrm{coh}}^{\sin\phi}$ and $A_{\mathrm{LU,I,coh}}^{\sin\phi}$.

In conclusion, even in the region $-t < 0.06\,\mathrm{GeV}^2$ where the coherent process contributes about 40%, all asymmetries on deuterium that have (approximate) counterparts for hydrogen are found to be compatible with them. The data are unable to reveal any evidence of the influence of the Compton form factor $\mathcal{H}_5$ or features of the deuteron Compton form factors $\mathcal{H}_1$ and $\widetilde{\mathcal{H}}_1$ that distinguish them from the counterparts for the proton. Hence, coherent scattering presents no obvious signature in these data. The deuteron Compton form factor $\mathcal{H}_1$ appears to have a similar behavior as $\mathcal{H}$ of the proton. The data were compared with theoretical calculations for only incoherent scattering, based on a well-known GPD model. Those asymmetries that are expected to resemble counterparts for a hydrogen target reveal the same shortcomings of the model calculations that appeared in comparisons with the hydrogen data.

9. Acknowledgments

We gratefully acknowledge the DESY management for its support and the staff at DESY and the collaborating institutions for their significant effort. This work was supported by the Ministry of Economy and the Ministry of Education and Science of Armenia; the FWO-Flanders and IWT, Belgium; the Natural Sciences and Engineering Research Council of Canada; the National Natural Science Foundation of China; the Alexander von Humboldt Stiftung, the German Bundesministerium für Bildung und Forschung (BMBF), and the Deutsche Forschungsgemeinschaft (DFG); the Italian Is-

tituto Nazionale di Fisica Nucleare (INFN); the MEXT, JSPS, and G-COE of Japan; the Dutch Foundation for Fundamenteel Onderzoek der Materie (FOM); the Russian Academy of Science and the Russian Federal Agency for Science and Innovations; the U.K. Engineering and Physical Sciences Research Council, the Science and Technology Facilities Council, and the Scottish Universities Physics Alliance; the U.S. Department of Energy (DOE) and the National Science Foundation (NSF); and the European Community Research Infrastructure Integrating Activity under the FP7 "Study of strongly interacting matter (HadronPhysics2, Grant Agreement number 227431)".

Table 5
Results for azimuthal Fourier amplitudes of the single-charge asymmetries $\mathcal{A}_{\mathrm{L}\overleftrightarrows}$, $\mathcal{A}_{\mathrm{UL}}$ and $\mathcal{A}_{\mathrm{LL}}$, extracted from longitudinally polarized deuteron data, for a tensor polarization of $P_{zz} = 0.827$. Not included are the 1.9%, 4.0% and 4.4% scale uncertainties for corresponding asymmetry amplitudes arising from the uncertainties in the measurement of the beam, target, beam and target polarizations, respectively.

Kinematic bin		$\langle -t \rangle$ [GeV^2]	$\langle x_N \rangle$	$\langle Q^2 \rangle$ [GeV^2]	$A_{\mathrm{L}\overleftrightarrows}^{\sin\phi}$ $\pm\delta_{\mathrm{stat}} \pm \delta_{\mathrm{syst}}$	$A_{\mathrm{L}\overleftrightarrows}^{\sin(2\phi)}$ $\pm\delta_{\mathrm{stat}} \pm \delta_{\mathrm{syst}}$	$A_{\mathrm{UL}}^{\sin\phi}$ $\pm\delta_{\mathrm{stat}} \pm \delta_{\mathrm{syst}}$	$A_{\mathrm{UL}}^{\sin(2\phi)}$ $\pm\delta_{\mathrm{stat}} \pm \delta_{\mathrm{syst}}$
	Overall	0.13	0.10	2.5	$-0.148 \pm 0.036 \pm 0.058$	$-0.012 \pm 0.035 \pm 0.013$	$-0.044 \pm 0.023 \pm 0.029$	$-0.037 \pm 0.022 \pm 0.010$
$-t$[GeV^2]	0.00-0.06	0.03	0.08	1.9	$-0.171 \pm 0.058 \pm 0.049$	$0.043 \pm 0.057 \pm 0.005$	$-0.018 \pm 0.037 \pm 0.031$	$-0.015 \pm 0.036 \pm 0.010$
	0.06-0.14	0.10	0.10	2.5	$-0.131 \pm 0.066 \pm 0.037$	$-0.053 \pm 0.065 \pm 0.010$	$-0.036 \pm 0.042 \pm 0.018$	$-0.094 \pm 0.041 \pm 0.013$
	0.14-0.30	0.20	0.11	2.9	$-0.246 \pm 0.074 \pm 0.025$	$0.032 \pm 0.075 \pm 0.007$	$-0.057 \pm 0.047 \pm 0.012$	$-0.006 \pm 0.048 \pm 0.015$
	0.30-0.70	0.42	0.12	3.5	$0.064 \pm 0.111 \pm 0.032$	$-0.217 \pm 0.115 \pm 0.008$	$-0.116 \pm 0.071 \pm 0.009$	$0.024 \pm 0.075 \pm 0.023$
x_N	0.03-0.07	0.11	0.05	1.4	$-0.093 \pm 0.058 \pm 0.064$	$0.018 \pm 0.060 \pm 0.035$	$-0.025 \pm 0.037 \pm 0.016$	$-0.034 \pm 0.038 \pm 0.005$
	0.07-0.10	0.11	0.08	2.1	$-0.140 \pm 0.067 \pm 0.062$	$-0.019 \pm 0.066 \pm 0.013$	$-0.046 \pm 0.042 \pm 0.026$	$-0.023 \pm 0.042 \pm 0.006$
	0.10-0.15	0.14	0.12	3.1	$-0.238 \pm 0.077 \pm 0.055$	$0.066 \pm 0.077 \pm 0.014$	$-0.037 \pm 0.049 \pm 0.026$	$-0.048 \pm 0.049 \pm 0.006$
	0.15-0.35	0.20	0.20	5.0	$-0.156 \pm 0.109 \pm 0.049$	$-0.165 \pm 0.103 \pm 0.013$	$-0.104 \pm 0.069 \pm 0.030$	$-0.036 \pm 0.068 \pm 0.009$
Q^2[GeV^2]	1.0-1.5	0.09	0.06	1.2	$-0.103 \pm 0.068 \pm 0.043$	$-0.017 \pm 0.067 \pm 0.051$	$-0.022 \pm 0.043 \pm 0.023$	$-0.004 \pm 0.042 \pm 0.005$
	1.5-2.3	0.11	0.08	1.9	$-0.169 \pm 0.065 \pm 0.047$	$0.065 \pm 0.066 \pm 0.032$	$-0.035 \pm 0.041 \pm 0.026$	$-0.071 \pm 0.042 \pm 0.006$
	2.3-3.5	0.14	0.11	2.8	$-0.110 \pm 0.074 \pm 0.050$	$-0.077 \pm 0.073 \pm 0.014$	$-0.091 \pm 0.047 \pm 0.026$	$-0.002 \pm 0.046 \pm 0.008$
	3.5-10.0	0.20	0.17	4.9	$-0.212 \pm 0.079 \pm 0.042$	$-0.036 \pm 0.080 \pm 0.006$	$-0.025 \pm 0.050 \pm 0.024$	$-0.073 \pm 0.050 \pm 0.008$

Kinematic bin		$\langle -t \rangle$ [GeV^2]	$\langle x_N \rangle$	$\langle Q^2 \rangle$ [GeV^2]	$A_{\mathrm{UL}}^{\sin(3\phi)}$ $\pm\delta_{\mathrm{stat}} \pm \delta_{\mathrm{syst}}$	$A_{\mathrm{LL}}^{\cos(0\phi)}$ $\pm\delta_{\mathrm{stat}} \pm \delta_{\mathrm{syst}}$	$A_{\mathrm{LL}}^{\cos\phi}$ $\pm\delta_{\mathrm{stat}} \pm \delta_{\mathrm{syst}}$	$A_{\mathrm{LL}}^{\cos(2\phi)}$ $\pm\delta_{\mathrm{stat}} \pm \delta_{\mathrm{syst}}$
	Overall	0.13	0.10	2.5	$-0.039 \pm 0.022 \pm 0.004$	$0.011 \pm 0.029 \pm 0.004$	$0.072 \pm 0.042 \pm 0.019$	$-0.017 \pm 0.042 \pm 0.005$
$-t$[GeV^2]	0.00-0.06	0.03	0.08	1.9	$0.009 \pm 0.036 \pm 0.005$	$0.012 \pm 0.048 \pm 0.005$	$0.136 \pm 0.066 \pm 0.010$	$-0.115 \pm 0.068 \pm 0.008$
	0.06-0.14	0.10	0.10	2.5	$-0.112 \pm 0.041 \pm 0.006$	$-0.011 \pm 0.055 \pm 0.007$	$0.013 \pm 0.076 \pm 0.011$	$0.002 \pm 0.077 \pm 0.009$
	0.14-0.30	0.20	0.11	2.9	$-0.045 \pm 0.047 \pm 0.006$	$-0.015 \pm 0.063 \pm 0.005$	$0.052 \pm 0.090 \pm 0.034$	$0.078 \pm 0.089 \pm 0.009$
	0.30-0.70	0.42	0.12	3.5	$0.060 \pm 0.074 \pm 0.014$	$0.200 \pm 0.099 \pm 0.010$	$0.136 \pm 0.147 \pm 0.068$	$0.143 \pm 0.139 \pm 0.005$
x_N	0.03-0.07	0.11	0.05	1.4	$-0.053 \pm 0.038 \pm 0.002$	$0.008 \pm 0.051 \pm 0.003$	$0.062 \pm 0.074 \pm 0.003$	$0.064 \pm 0.070 \pm 0.003$
	0.07-0.10	0.11	0.08	2.1	$0.006 \pm 0.041 \pm 0.004$	$-0.011 \pm 0.056 \pm 0.007$	$0.108 \pm 0.078 \pm 0.014$	$-0.085 \pm 0.079 \pm 0.005$
	0.10-0.15	0.14	0.12	3.1	$-0.011 \pm 0.047 \pm 0.004$	$0.043 \pm 0.064 \pm 0.014$	$-0.004 \pm 0.090 \pm 0.021$	$-0.112 \pm 0.088 \pm 0.009$
	0.15-0.35	0.20	0.20	5.0	$-0.142 \pm 0.066 \pm 0.011$	$-0.003 \pm 0.091 \pm 0.024$	$0.199 \pm 0.128 \pm 0.034$	$0.065 \pm 0.126 \pm 0.017$
Q^2[GeV^2]	1.0-1.5	0.09	0.06	1.2	$-0.037 \pm 0.042 \pm 0.004$	$-0.062 \pm 0.056 \pm 0.006$	$0.008 \pm 0.078 \pm 0.009$	$0.083 \pm 0.080 \pm 0.007$
	1.5-2.3	0.11	0.08	1.9	$-0.006 \pm 0.041 \pm 0.006$	$0.054 \pm 0.055 \pm 0.005$	$0.047 \pm 0.079 \pm 0.010$	$-0.150 \pm 0.078 \pm 0.007$
	2.3-3.5	0.14	0.11	2.8	$-0.047 \pm 0.046 \pm 0.003$	$0.001 \pm 0.061 \pm 0.006$	$0.103 \pm 0.085 \pm 0.007$	$0.027 \pm 0.086 \pm 0.007$
	3.5-10.0	0.20	0.17	4.9	$-0.069 \pm 0.050 \pm 0.005$	$0.045 \pm 0.067 \pm 0.016$	$0.166 \pm 0.095 \pm 0.010$	$-0.011 \pm 0.095 \pm 0.007$

Table 6
Results for azimuthal Fourier amplitudes of the single-beam-helicity charge asymmetry $\mathcal{A}_{C\overleftarrow{\Leftarrow}}$, extracted from longitudinally polarized deuteron data, for $P_\ell = -0.530$ and a tensor polarization of $\overleftarrow{\overrightarrow{P}}_{zz} = 0.827$. Not included is the 2.2% scale uncertainty for $\sin(n\phi)$ asymmetry amplitudes arising from the uncertainty in the measurement of the beam polarization.

Kinematic bin		$\langle -t \rangle$ [GeV^2]	$\langle x_N \rangle$	$\langle Q^2 \rangle$ [GeV^2]	$A^{\cos(0\phi)}_{C\overleftarrow{\Leftarrow}}$ $\pm\delta_{\rm stat} \pm \delta_{\rm syst}$	$A^{\cos\phi}_{C\overleftarrow{\Leftarrow}}$ $\pm\delta_{\rm stat} \pm \delta_{\rm syst}$	$A^{\cos(2\phi)}_{C\overleftarrow{\Leftarrow}}$ $\pm\delta_{\rm stat} \pm \delta_{\rm syst}$
Overall		0.13	0.10	2.5	$-0.012 \pm 0.018 \pm 0.034$	$0.065 \pm 0.026 \pm 0.009$	$0.017 \pm 0.026 \pm 0.003$
$-t$[GeV^2]	0.00-0.06	0.03	0.08	1.9	$0.006 \pm 0.030 \pm 0.031$	$0.001 \pm 0.041 \pm 0.012$	$0.005 \pm 0.042 \pm 0.009$
	0.06-0.14	0.10	0.10	2.5	$0.074 \pm 0.035 \pm 0.034$	$0.037 \pm 0.049 \pm 0.008$	$0.046 \pm 0.049 \pm 0.006$
	0.14-0.30	0.20	0.11	2.9	$-0.098 \pm 0.036 \pm 0.031$	$0.139 \pm 0.052 \pm 0.008$	$-0.007 \pm 0.051 \pm 0.005$
	0.30-0.70	0.42	0.12	3.5	$-0.086 \pm 0.058 \pm 0.028$	$0.159 \pm 0.088 \pm 0.007$	$0.056 \pm 0.079 \pm 0.008$
x_N	0.03-0.07	0.11	0.05	1.4	$-0.046 \pm 0.031 \pm 0.035$	$0.042 \pm 0.044 \pm 0.009$	$-0.078 \pm 0.043 \pm 0.005$
	0.07-0.10	0.11	0.08	2.1	$0.025 \pm 0.035 \pm 0.030$	$0.005 \pm 0.050 \pm 0.005$	$0.071 \pm 0.048 \pm 0.003$
	0.10-0.15	0.14	0.12	3.1	$0.007 \pm 0.040 \pm 0.028$	$0.038 \pm 0.055 \pm 0.010$	$0.034 \pm 0.055 \pm 0.004$
	0.15-0.35	0.20	0.20	5.0	$-0.052 \pm 0.054 \pm 0.024$	$0.194 \pm 0.077 \pm 0.018$	$0.091 \pm 0.079 \pm 0.004$
Q^2[GeV^2]	1.0-1.5	0.09	0.06	1.2	$-0.059 \pm 0.034 \pm 0.039$	$0.119 \pm 0.047 \pm 0.007$	$0.019 \pm 0.049 \pm 0.006$
	1.5-2.3	0.11	0.08	1.9	$0.002 \pm 0.034 \pm 0.034$	$0.004 \pm 0.049 \pm 0.004$	$-0.023 \pm 0.047 \pm 0.002$
	2.3-3.5	0.14	0.11	2.8	$0.012 \pm 0.038 \pm 0.028$	$0.034 \pm 0.053 \pm 0.005$	$0.087 \pm 0.054 \pm 0.004$
	3.5-10.0	0.20	0.17	4.9	$-0.005 \pm 0.041 \pm 0.022$	$0.111 \pm 0.058 \pm 0.010$	$-0.004 \pm 0.058 \pm 0.005$

Kinematic bin		$\langle -t \rangle$ [GeV^2]	$\langle x_N \rangle$	$\langle Q^2 \rangle$ [GeV^2]	$A^{\cos(3\phi)}_{C\overleftarrow{\Leftarrow}}$ $\pm\delta_{\rm stat} \pm \delta_{\rm syst}$	$A^{\sin\phi}_{C\overleftarrow{\Leftarrow}}$ $\pm\delta_{\rm stat} \pm \delta_{\rm syst}$	$A^{\sin(2\phi)}_{C\overleftarrow{\Leftarrow}}$ $\pm\delta_{\rm stat} \pm \delta_{\rm syst}$
Overall		0.13	0.10	2.5	$0.044 \pm 0.026 \pm 0.003$	$-0.123 \pm 0.049 \pm 0.057$	$0.036 \pm 0.049 \pm 0.020$
$-t$[GeV^2]	0.00-0.06	0.03	0.08	1.9	$-0.018 \pm 0.042 \pm 0.004$	$-0.158 \pm 0.081 \pm 0.050$	$0.109 \pm 0.080 \pm 0.005$
	0.06-0.14	0.10	0.10	2.5	$0.075 \pm 0.049 \pm 0.004$	$-0.156 \pm 0.095 \pm 0.036$	$-0.021 \pm 0.094 \pm 0.015$
	0.14-0.30	0.20	0.11	2.9	$0.053 \pm 0.052 \pm 0.005$	$-0.126 \pm 0.098 \pm 0.021$	$0.018 \pm 0.099 \pm 0.011$
	0.30-0.70	0.42	0.12	3.5	$0.098 \pm 0.077 \pm 0.007$	$0.141 \pm 0.142 \pm 0.029$	$-0.015 \pm 0.153 \pm 0.015$
x_N	0.03-0.07	0.11	0.05	1.4	$-0.002 \pm 0.041 \pm 0.002$	$-0.109 \pm 0.080 \pm 0.060$	$-0.028 \pm 0.081 \pm 0.039$
	0.07-0.10	0.11	0.08	2.1	$0.028 \pm 0.049 \pm 0.003$	$-0.069 \pm 0.092 \pm 0.059$	$0.095 \pm 0.094 \pm 0.018$
	0.10-0.15	0.14	0.12	3.1	$0.091 \pm 0.056 \pm 0.006$	$-0.288 \pm 0.107 \pm 0.058$	$0.119 \pm 0.107 \pm 0.018$
	0.15-0.35	0.20	0.20	5.0	$0.089 \pm 0.075 \pm 0.005$	$-0.032 \pm 0.147 \pm 0.054$	$-0.020 \pm 0.141 \pm 0.011$
Q^2[GeV^2]	1.0-1.5	0.09	0.06	1.2	$-0.020 \pm 0.048 \pm 0.002$	$0.020 \pm 0.095 \pm 0.041$	$0.011 \pm 0.092 \pm 0.056$
	1.5-2.3	0.11	0.08	1.9	$0.074 \pm 0.047 \pm 0.003$	$-0.266 \pm 0.087 \pm 0.043$	$0.095 \pm 0.092 \pm 0.038$
	2.3-3.5	0.14	0.11	2.8	$0.076 \pm 0.053 \pm 0.006$	$-0.076 \pm 0.101 \pm 0.053$	$-0.023 \pm 0.099 \pm 0.016$
	3.5-10.0	0.20	0.17	4.9	$0.059 \pm 0.058 \pm 0.003$	$-0.145 \pm 0.112 \pm 0.044$	$0.042 \pm 0.112 \pm 0.011$

Table 7
Results for azimuthal Fourier amplitudes of the single-beam-helicity charge-averaged asymmetry $\mathcal{A}_{\overset{0}{\leftarrow}\mathrm{L}}$, extracted from longitudinally polarized deuteron data, for $P_\ell = -0.530$ and a tensor polarization of $P_{zz} = 0.827$. Not included is the 5.3% (5.7%) scale uncertainty for the $\sin(n\phi)$ ($\cos(n\phi)$) asymmetry amplitudes arising from the uncertainties in the measurement of the target (beam and target) polarizations.

Kinematic bin		$\langle -t \rangle$ [GeV^2]	$\langle x_N \rangle$	$\langle Q^2 \rangle$ [GeV^2]	$A^{\cos(0\phi)}_{\overset{0}{\leftarrow}\mathrm{L}}$ $\pm\delta_{\mathrm{stat}} \pm \delta_{\mathrm{syst}}$	$A^{\cos\phi}_{\overset{0}{\leftarrow}\mathrm{L}}$ $\pm\delta_{\mathrm{stat}} \pm \delta_{\mathrm{syst}}$	$A^{\sin\phi}_{\overset{0}{\leftarrow}\mathrm{L}}$ $\pm\delta_{\mathrm{stat}} \pm \delta_{\mathrm{syst}}$	$A^{\sin(2\phi)}_{\overset{0}{\leftarrow}\mathrm{L}}$ $\pm\delta_{\mathrm{stat}} \pm \delta_{\mathrm{syst}}$
Overall		0.13	0.10	2.5	$0.021 \pm 0.044 \pm 0.009$	$-0.041 \pm 0.062 \pm 0.010$	$0.005 \pm 0.033 \pm 0.003$	$-0.036 \pm 0.033 \pm 0.003$
$-t$[GeV^2]	0.00-0.06	0.03	0.08	1.9	$-0.009 \pm 0.072 \pm 0.008$	$0.087 \pm 0.101 \pm 0.011$	$0.011 \pm 0.054 \pm 0.004$	$0.033 \pm 0.054 \pm 0.005$
	0.06-0.14	0.10	0.10	2.5	$0.039 \pm 0.083 \pm 0.012$	$-0.005 \pm 0.115 \pm 0.011$	$0.003 \pm 0.063 \pm 0.006$	$-0.108 \pm 0.062 \pm 0.006$
	0.14-0.30	0.20	0.11	2.9	$0.030 \pm 0.091 \pm 0.008$	$-0.282 \pm 0.128 \pm 0.024$	$0.058 \pm 0.068 \pm 0.003$	$-0.034 \pm 0.068 \pm 0.005$
	0.30-0.70	0.42	0.12	3.5	$0.024 \pm 0.142 \pm 0.014$	$-0.056 \pm 0.206 \pm 0.059$	$-0.137 \pm 0.100 \pm 0.008$	$-0.093 \pm 0.111 \pm 0.011$
x_N	0.03-0.07	0.11	0.05	1.4	$0.051 \pm 0.075 \pm 0.004$	$-0.121 \pm 0.106 \pm 0.005$	$-0.001 \pm 0.054 \pm 0.002$	$-0.008 \pm 0.056 \pm 0.002$
	0.07-0.10	0.11	0.08	2.1	$-0.014 \pm 0.083 \pm 0.012$	$-0.049 \pm 0.117 \pm 0.021$	$0.020 \pm 0.062 \pm 0.004$	$-0.043 \pm 0.062 \pm 0.006$
	0.10-0.15	0.14	0.12	3.1	$-0.158 \pm 0.095 \pm 0.019$	$0.033 \pm 0.133 \pm 0.030$	$0.093 \pm 0.072 \pm 0.006$	$-0.029 \pm 0.071 \pm 0.006$
	0.15-0.35	0.20	0.20	5.0	$0.228 \pm 0.135 \pm 0.027$	$0.093 \pm 0.187 \pm 0.044$	$-0.108 \pm 0.100 \pm 0.011$	$-0.069 \pm 0.095 \pm 0.011$
Q^2[GeV^2]	1.0-1.5	0.09	0.06	1.2	$0.028 \pm 0.085 \pm 0.009$	$-0.108 \pm 0.116 \pm 0.013$	$-0.011 \pm 0.065 \pm 0.008$	$0.019 \pm 0.065 \pm 0.005$
	1.5-2.3	0.11	0.08	1.9	$-0.029 \pm 0.082 \pm 0.006$	$-0.077 \pm 0.119 \pm 0.009$	$-0.025 \pm 0.059 \pm 0.005$	$-0.140 \pm 0.061 \pm 0.005$
	2.3-3.5	0.14	0.11	2.8	$0.018 \pm 0.091 \pm 0.012$	$-0.049 \pm 0.125 \pm 0.013$	$0.047 \pm 0.069 \pm 0.004$	$-0.011 \pm 0.066 \pm 0.005$
	3.5-10.0	0.20	0.17	4.9	$0.078 \pm 0.100 \pm 0.022$	$0.127 \pm 0.142 \pm 0.020$	$0.024 \pm 0.075 \pm 0.005$	$-0.013 \pm 0.075 \pm 0.007$

Table 8
Results for azimuthal Fourier amplitudes of the single-beam-helicity beam-charge⊗target-spin asymmetry $\mathcal{A}_{\overleftarrow{\mathrm{L}}}^{\mathrm{C}}$, extracted from longitudinally polarized deuteron data, for $P_\ell = -0.530$ and a tensor polarization of $P_{zz} = 0.827$. Not included is the 5.3% (5.7%) scale uncertainty for the $\sin(n\phi)$ ($\cos(n\phi)$) asymmetry amplitudes arising from the uncertainties in the measurement of the target (beam and target) polarizations.

Kinematic bin		$\langle -t \rangle$ [GeV^2]	$\langle x_N \rangle$	$\langle Q^2 \rangle$ [GeV^2]	$A_{\overleftarrow{\mathrm{L}}}^{\cos(0\phi)}$ $\pm\delta_{\mathrm{stat}} \pm \delta_{\mathrm{syst}}$	$A_{\overleftarrow{\mathrm{L}}}^{\cos\phi}$ $\pm\delta_{\mathrm{stat}} \pm \delta_{\mathrm{syst}}$	$A_{\overleftarrow{\mathrm{L}}}^{\cos(2\phi)}$ $\pm\delta_{\mathrm{stat}} \pm \delta_{\mathrm{syst}}$
Overall		0.13	0.10	2.5	$-0.082 \pm 0.044 \pm 0.002$	$0.148 \pm 0.062 \pm 0.007$	$-0.044 \pm 0.057 \pm 0.002$
$-t$[GeV^2]	0.00-0.06	0.03	0.08	1.9	$-0.089 \pm 0.072 \pm 0.002$	$0.124 \pm 0.100 \pm 0.006$	$-0.161 \pm 0.095 \pm 0.003$
	0.06-0.14	0.10	0.10	2.5	$-0.071 \pm 0.082 \pm 0.002$	$0.147 \pm 0.114 \pm 0.007$	$-0.225 \pm 0.110 \pm 0.006$
	0.14-0.30	0.20	0.11	2.9	$-0.152 \pm 0.091 \pm 0.003$	$0.262 \pm 0.127 \pm 0.008$	$0.092 \pm 0.114 \pm 0.005$
	0.30-0.70	0.42	0.12	3.5	$0.190 \pm 0.142 \pm 0.014$	$0.244 \pm 0.205 \pm 0.006$	$0.547 \pm 0.172 \pm 0.014$
x_N	0.03-0.07	0.11	0.05	1.4	$-0.044 \pm 0.075 \pm 0.003$	$0.101 \pm 0.109 \pm 0.001$	$0.019 \pm 0.093 \pm 0.003$
	0.07-0.10	0.11	0.08	2.1	$-0.170 \pm 0.082 \pm 0.004$	$0.210 \pm 0.116 \pm 0.006$	$-0.132 \pm 0.108 \pm 0.003$
	0.10-0.15	0.14	0.12	3.1	$0.058 \pm 0.095 \pm 0.002$	$0.323 \pm 0.132 \pm 0.010$	$-0.239 \pm 0.123 \pm 0.007$
	0.15-0.35	0.20	0.20	5.0	$-0.281 \pm 0.135 \pm 0.012$	$-0.045 \pm 0.188 \pm 0.009$	$0.269 \pm 0.173 \pm 0.012$
Q^2[GeV^2]	1.0-1.5	0.09	0.06	1.2	$-0.100 \pm 0.085 \pm 0.002$	$-0.016 \pm 0.116 \pm 0.001$	$-0.032 \pm 0.108 \pm 0.005$
	1.5-2.3	0.11	0.08	1.9	$-0.097 \pm 0.082 \pm 0.002$	$0.140 \pm 0.119 \pm 0.005$	$-0.069 \pm 0.104 \pm 0.003$
	2.3-3.5	0.14	0.11	2.8	$-0.002 \pm 0.089 \pm 0.001$	$0.483 \pm 0.123 \pm 0.010$	$-0.068 \pm 0.120 \pm 0.002$
	3.5-10.0	0.20	0.17	4.9	$-0.145 \pm 0.100 \pm 0.003$	$-0.003 \pm 0.141 \pm 0.008$	$0.005 \pm 0.131 \pm 0.009$

Kinematic bin		$\langle -t \rangle$ [GeV^2]	$\langle x_N \rangle$	$\langle Q^2 \rangle$ [GeV^2]	$A_{\overleftarrow{\mathrm{L}}}^{\sin\phi}$ $\pm\delta_{\mathrm{stat}} \pm \delta_{\mathrm{syst}}$	$A_{\overleftarrow{\mathrm{L}}}^{\sin(2\phi)}$ $\pm\delta_{\mathrm{stat}} \pm \delta_{\mathrm{syst}}$	$A_{\overleftarrow{\mathrm{L}}}^{\sin(3\phi)}$ $\pm\delta_{\mathrm{stat}} \pm \delta_{\mathrm{syst}}$
Overall		0.13	0.10	2.5	$-0.023 \pm 0.033 \pm 0.028$	$-0.035 \pm 0.033 \pm 0.008$	$-0.009 \pm 0.030 \pm 0.003$
$-t$[GeV^2]	0.00-0.06	0.03	0.08	1.9	$-0.032 \pm 0.054 \pm 0.033$	$-0.116 \pm 0.053 \pm 0.007$	$-0.064 \pm 0.050 \pm 0.004$
	0.06-0.14	0.10	0.10	2.5	$0.016 \pm 0.062 \pm 0.016$	$-0.016 \pm 0.062 \pm 0.009$	$-0.033 \pm 0.059 \pm 0.005$
	0.14-0.30	0.20	0.11	2.9	$-0.045 \pm 0.068 \pm 0.010$	$0.024 \pm 0.067 \pm 0.015$	$0.025 \pm 0.060 \pm 0.008$
	0.30-0.70	0.42	0.12	3.5	$-0.001 \pm 0.102 \pm 0.005$	$0.212 \pm 0.115 \pm 0.020$	$0.201 \pm 0.099 \pm 0.008$
x_N	0.03-0.07	0.11	0.05	1.4	$-0.027 \pm 0.054 \pm 0.015$	$0.006 \pm 0.058 \pm 0.005$	$-0.007 \pm 0.051 \pm 0.001$
	0.07-0.10	0.11	0.08	2.1	$-0.073 \pm 0.061 \pm 0.023$	$-0.098 \pm 0.062 \pm 0.004$	$0.001 \pm 0.057 \pm 0.003$
	0.10-0.15	0.14	0.12	3.1	$0.031 \pm 0.072 \pm 0.026$	$-0.087 \pm 0.072 \pm 0.003$	$0.025 \pm 0.065 \pm 0.003$
	0.15-0.35	0.20	0.20	5.0	$0.009 \pm 0.100 \pm 0.031$	$-0.001 \pm 0.097 \pm 0.002$	$-0.036 \pm 0.090 \pm 0.006$
Q^2[GeV^2]	1.0-1.5	0.09	0.06	1.2	$-0.003 \pm 0.065 \pm 0.022$	$0.020 \pm 0.065 \pm 0.003$	$-0.003 \pm 0.058 \pm 0.001$
	1.5-2.3	0.11	0.08	1.9	$-0.064 \pm 0.059 \pm 0.026$	$-0.041 \pm 0.061 \pm 0.004$	$-0.017 \pm 0.057 \pm 0.005$
	2.3-3.5	0.14	0.11	2.8	$-0.087 \pm 0.068 \pm 0.021$	$-0.090 \pm 0.065 \pm 0.008$	$-0.014 \pm 0.062 \pm 0.001$
	3.5-10.0	0.20	0.17	4.9	$0.102 \pm 0.075 \pm 0.027$	$-0.040 \pm 0.075 \pm 0.005$	$-0.004 \pm 0.070 \pm 0.004$

References

[1] D. Müller et al., Fortschr. Phys. **42** (1994) 101.
[2] A.V. Radyushkin, Phys. Lett. **B380** (1996) 417.
A.V. Radyushkin, Phys. Rev. **D56** (1997) 5524.
[3] X. Ji, Phys. Rev. Lett. **78** (1997) 610.
X. Ji, Phys. Rev. **D55** (1997) 7114.
[4] J.P. Ralston and B. Pire, Phys. Rev. **D66** (2002) 111501.
[5] M. Burkardt, Phys. Rev. **D62** (2000) 071503; Erratum-ibid **D66** (2002) 119903.
M. Burkardt, Int. J. Mod. Phys. **A18** (2003) 173.
[6] M. Diehl, Eur. Phys. J. **C25** (2002) 223; Erratum-ibid **C31** (2003) 277.
[7] A.V. Belitsky and D. Müller, Nucl. Phys. **A711** (2002) 118.
[8] M. Diehl, Phys. Rept. **388** (2003) 41.
[9] A.V. Belitsky and A.V. Radyushkin, Phys. Rept. **418** (2005) 1.
[10] J. Blümlein, B. Geyer, and D. Robaschik, Nucl. Phys. **B560** (1999) 283.
[11] A.V. Belitsky and D. Müller, Nucl. Phys. **B537** (1999) 397.
[12] A.V. Belitsky, A. Freund and D. Müller, Nucl. Phys. **B574** (2000) 347.
[13] A.V. Belitsky and D. Müller, Phys. Lett. **B486** (2000) 369.
[14] I.V. Anikin and O.V. Teryaev, Phys. Rev. **D76** (2007) 056007.
[15] K. Kumericki, D. Müller, and K. Passek-Kumericki, Eur. Phys. J. **C58** (2008) 193.
[16] A.V. Belitsky, D. Müller, and A. Kirchner, Nucl. Phys. **B629** (2002) 323.
[17] E.R. Berger, F. Cano, M. Diehl, and B. Pire, Phys. Rev. Lett. **87** (2001) 142302.
[18] A. Kirchner and D. Müller, Eur. Phys. J. **C32** (2004) 347.
[19] F. Cano and B. Pire, Eur. Phys. J. **A19** (2004) 423.
[20] HERMES Collaboration, A. Airapetian et al., Phys. Rev. Lett. **95** (2005) 242001.
[21] HERMES Collaboration, A. Airapetian et al., Phys. Rev. **D75** (2007) 012007.
[22] M. Lacombe et al., Phys. Lett. **B101** (1981) 139.
[23] B. Krauss, Ph. D. thesis, Friedrich-Alexander Universität Erlangen-Nürnberg, Germany, February 2005, DESY-THESIS-2005-008.
[24] HERMES Collaboration, A. Airapetian et al., JHEP **06** (2010) 019.
[25] M. Diehl, T. Gousset, B. Pire, and J.P. Ralston, Phys. Lett. **B411** (1997) 193.
[26] HERMES Collaboration, A. Airapetian et al., JHEP **11** (2009) 083.
[27] HERMES Collaboration, A. Airapetian et al., Nucl. Phys. **B829** (2010) 1.
[28] JLAB t20 Collaboration, D. Abbott et al., Eur. Phys. J. **A7** (2000) 421.
[29] A. Bacchetta, U. D'Alesio, M Diehl and C.A. Miller, Phys. Rev. **D70** (2004) 117504.
[30] HERMES Collaboration, K. Ackerstaff et al., Nucl. Instr. and Meth. **A417** (1998) 230.
[31] A. Sokolov and I. Ternov, Sov. Phys. Doklady **8** (1964) 1203.
[32] J. Buon and K. Steffen, Nucl. Instr. and Meth. **A245** (1986) 248.
[33] D.P. Barber et al., Nucl. Instr. and Meth. **A338** (1994) 166.
[34] M. Beckmann et al., Nucl. Instr. and Meth. **A479** (2002) 334.
[35] A. Nass et al., Nucl. Instr. and Meth. **A505** (2003) 633.
[36] C. Baumgarten et al., Nucl. Instr. and Meth. **A496** (2003) 606.
[37] C. Baumgarten et al., Nucl. Instr. and Meth. **A508** (2003) 268.
[38] HERMES Collaboration, A. Airapetian et al., Nucl. Instr. and Meth. **A540** (2005) 68.
[39] F. Ellinghaus, Ph. D. thesis, Humboldt Universität Berlin, Germany, January 2004, DESY-THESIS-2004-005.
[40] HERMES Collaboration, A. Airapetian et al., Phys. Rev. **D75** (2007) 011103.
[41] R. Barlow, Nucl. Instr. and Meth. **A297** (1990) 496.
[42] HERMES Collaboration, A. Airapetian et al., JHEP **06** (2008) 066.
[43] A. Vandenbroucke, Ph. D. thesis, Universiteit Gent, Belgium, November 2006, DESY-THESIS-2007-003.
[44] V.A. Korotkov and W.D. Nowak, Eur. Phys. J. **C23** (2002) 455.
[45] M. Vanderhaeghen, P.A.M. Guichon, and M. Guidal, Phys. Rev. **D60** (1999) 094017.
[46] A.V. Afanasev, M.I. Konchatnij, and N.P. Merenkov, J. Exp. Theor. Phys. **102** (2006) 220.
[47] A. Umnikov, L. Kaptari, K. Kazakov, and F. Khanna, University of Alberta Report No. Alberta-Thy-29-94 (1994), hep-ph/9410241.

[48] M. Vanderhaeghen, P.A.M. Guichon, and M. Guidal, Computer code for the calculation of DVCS and BH processes in the reaction $ep \to ep\gamma$, private communication, 2007.
[49] K. Goeke, M.V. Polyakov, and M. Vanderhaeghen, Prog. Part. Nucl. Phys. **47** (2001) 401.
[50] L.V. Musatov and A.V. Radyushkin, Phys. Rev. **D61** (2000) 074027.